CHAPTER 4 RESULTS AND DISCUSSIONS

4.1 INTRODUCTION

This research project is focused on the synthesis and characterization of copper(II) mixed carboxylates of general formula $[Cu_2(p\text{-}H_2NC_6H_4COO)_n(CH_3(CH_2)_{14}COO)_{4\text{-}n}]$, where $n = 1 - 3$. These mixed carboxylates were specially designed to be low-temperature and thermally stable magnetic and redox-active metallomesogens.

In designing these complexes, three strategies were explored. The first strategy was to allow for self-assembly of the mesogens through H-bonding and Van der Waals forces. For this, the ligands chosen have $-NH_2$ group ($p\text{-}H_2NC_6H_4COO$) and long alkyl chains ($CH_3(CH_2)_{14}COO^-$).

The second strategy was to use the most suitable method for the synthesis of these complexes. In this research, the chosen method was the one-pot reaction [1,6] involving different copper(II) salts to find the optimum conditions (in terms of product and yield) to first prepare the more symmetrical complex ($n = 2$). This is based on the literature reports which used different copper(II) salts in the synthesis of homocarboxylate complexes [1-5]. Then, the less symmetrical complexes ($n = 1, 3$) were prepared using copper(II) acetate as this salt was preferred by many authors.

Chart 4.1 shows how these complexes were characterized.

Analyses		
	Chemical formula	→ CHN elemental analyses
	Structural formula	→ FTIR and UV-vis spectroscopies, molar conductivity
	Thermal stability	→ Thermogravimetry
	Phase transition	→ Differential scanning calorimetry
	Optical texture	→ Plane polarized optical microscopy
	Magnetism	→ Magnetic susceptibility
	Redox properties	→ Cyclic voltammetry
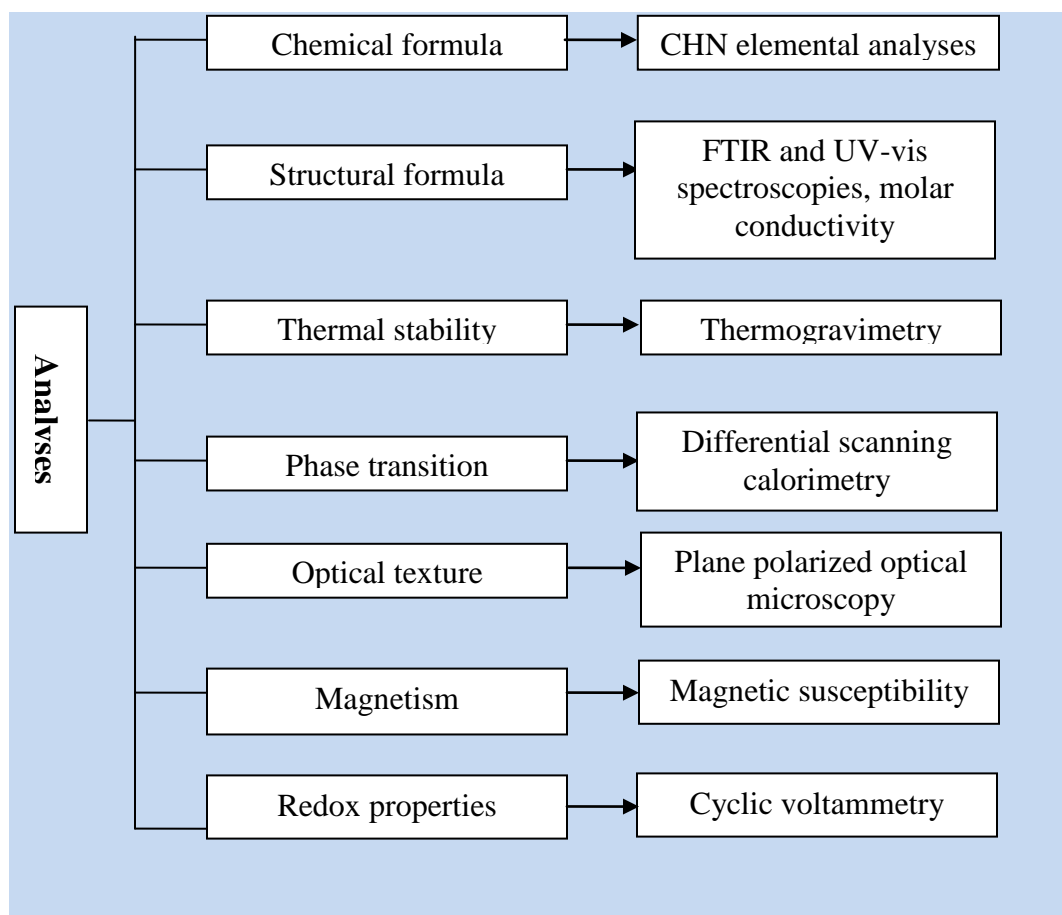
Chart 4.1 *Characterisation of complexes*

4.2. [Cu$_2$(*p*-H$_2$NC$_6$H$_4$COO)$_2$(CH$_3$(CH$_2$)$_{14}$COO)$_2$]

The one-pot synthesis involved mixing equimolar ratio of Cu(II) salt (anion = NO$_3^-$, CH$_3$COO$^-$, SO$_4^{2-}$, Cl$^-$), *p*-H$_2$NC$_6$H$_4$COOH and CH$_3$(CH$_2$)$_{14}$COOH in ethanol followed by neutralization with NH$_3$.

In the reaction, Cu^{2+} ion self-assembled with *p*-H$_2$NC$_6$H$_4$COO$^-$ and CH$_3$(CH$_2$)$_{14}$COO$^-$ ions, generated *in-situ* by NH$_3$ from the corresponding carboxylic acids. The general equation for the expected reaction is:

$$2\ Cu^{2+} + 2\ p\text{-}H_2NC_6H_4COOH + 2\ CH_3(CH_2)_{14}COOH$$

$$\Big\downarrow \begin{array}{l} NH_3 \\ EtOH,\ \Delta \end{array}$$

$$[Cu_2(p\text{-}H_3NC_6H_4COO)_2(CH_3(CH_2)_{14}COO)_2]$$
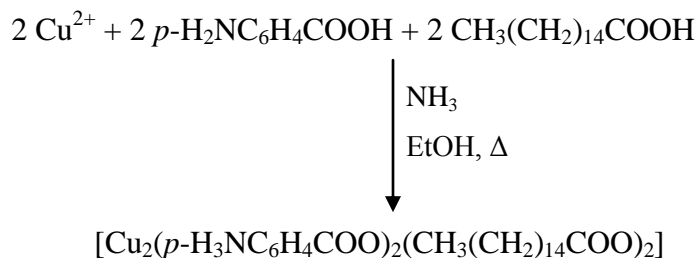
4.2.1 Reaction between $Cu(NO_3)_2$, $p\text{-}H_2NC_6H_4COOH$ and $CH_3(CH_2)_{14}COOH$

Two products were isolated from the reaction between $Cu(NO_3)_2$, $p\text{-}H_2NC_6H_4COOH$ and $CH_3(CH_2)_{14}COOH$: a pale blue powder (45.1%) and a dark green powder (41.5%).

(i) Pale blue powder

The pale blue powder (**Complex 1**) was the residue which deposited from the hot reaction mixture. It was soluble in ethanoic acid and pyridine, but insoluble in most other common polar and non-polar organic solvents. This is consistent with the presence of basic NH_2 group of the aromatic carboxylate, and suggests low polarity and/or absence of free coordination site.

The CHN elemental analyses (59.24% C, 10.92% H, 2.48% N) are in good agreement with the chemical formula $Cu_2C_{48}H_{82}N_2O_{10}$ (FW = 974.3 g mol^{-1}; 59.17% C, 8.48% H and 2.88% N). Based on the following evidence, the proposed chemical formula for **Complex 1** is [$Cu_2(p\text{-}H_2NC_6H_4COO)_2(CH_3(CH_2)_{14}COO)_2(H_2O)(CH_3CH_2OH)$], which is the intended product from the reaction.

The FTIR spectrum (**Figure 4.1**) of **Complex 1** show the presence of the expected functional groups based on the proposed structural formula, namely NH_2 at about 3200-3067 cm^{-1}, CH_2 at 2913 cm^{-1} (asymmetrical stretching) and 2848

cm^{-1} (symmetrical stretching), aromatic C-C at 1597 cm^{-1}, COO at 1597 and 1534 cm^{-1} (asymmetrical stretching), 1445 and 1406 cm^{-1} (symmetrical stretching), and *p*-substituted aromatic ring at 716 cm^{-1}. Accordingly, the ΔCOO values (ΔCOO = υ_{asym}COO − υ_{sym}COO) are 89 cm^{-1} (chelating) and 191 (monodentate *syn,anti*-bridging) for the carboxylate ligands [6]. These values suggest a binuclear complex.
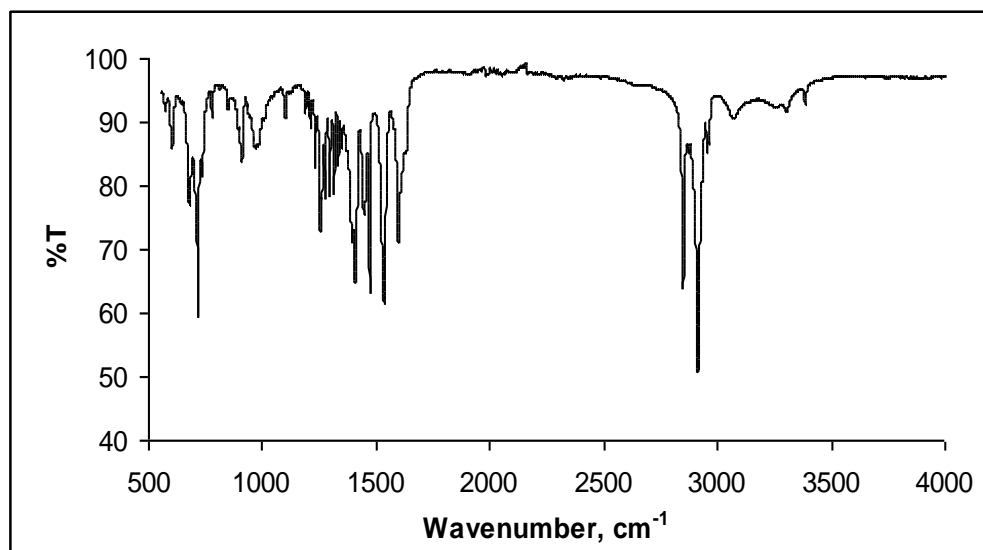
Figure 4.1 *The FTIR spectrum of **Complex 1***

The molar conductivity (Λ_M) of **Complex 1,** dissolved in DMSO-CH$_3$COOH is 21.2 S cm^2 mol^{-1}. The low value means that the complex is a non-electrolyte [7]. From this, it may be inferred that the complex did not dissociate to the corresponding ions in the mixed solvents. This fact is important when discussing the solution chemistry of the complex later.

The solid state electronic spectrum of **Complex 1** (**Figure 4.2(a)**) shows two broad *d-d* bands at 656 nm (Band I) and 441 nm (Band II) with absorbance

ratio ~ 3:1. This suggest either distorted square planar or square pyramidal binuclear Cu(II) complex [8-15].
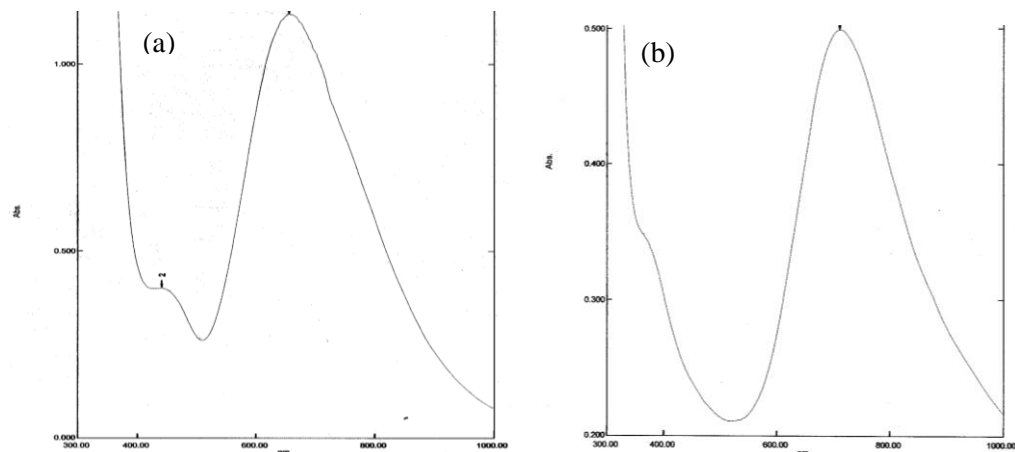
Figure 4.2 *The electronic spectrum of **Complex 1** as (a) a solid, and (b) solution (DMSO:CH$_3$COOH)*

In order to obtain useful information about this complex, its electronic spectroscopic data was compared with its "precursors", namely [Cu$_2$(p-H$_2$NC$_6$H$_4$COO)$_4$] and [Cu$_2$(CH$_3$(CH$_2$)$_{14}$COO)$_4$] (**Table 4.1**).

Table 4.1 *Solid electronic spectroscopic data of **Complex 1** and its "precursors"*

Complex	d-d Band (nm)		Absorbance ratio
	Band I	Band II	
Complex 1*	656	441	3:1
[Cu$_2$(p-H$_2$NC$_6$H$_4$COO)$_4$]	628	441	1:1
[Cu$_2$(CH$_3$(CH$_2$)$_{14}$COO)$_4$]	674	383	3:1

* [Cu$_2$(p-H$_2$NC$_6$H$_4$COO)$_2$(CH$_3$(CH$_2$)$_{14}$COO)$_2$(H$_2$O)(CH$_3$CH$_2$OH)]

Two deductions may be made from **Table 4.1**: (a) Band I of **Complex 1** is at intermediate energy between its "precursors". This supports the presence of

both aromatic and aliphatic carboxylates in the complex; and (b) Band II is at the same energy with the aromatic precursor, which are at lower energy compared to the aliphatic precursor. These suggests that the aromatic carboxylate is "closer" to Cu(II) compared to the aliphatic carboxylate.

The electronic spectrum of **Complex 1** (**Figure 4.2(b)**) dissolved in DMSO (with two drops of ethanoic acid added to increase its solubility) shows a broad d-d peak at 712 nm ($\varepsilon = 485$ M^{-1} cm^{-1}) and a distinct shoulder at 359 nm ($\varepsilon = 341$ M^{-1} cm^{-1}) superimposed on a strong charge-transfer band. The shoulder band is a characteristic of pentacoordinated binuclear complexes [8,10,12-15], in agreement with the proposed structure. It is also noted that the ε values for most mononuclear Cu(II) complexes are about 100 M^{-1} cm^{-1} [8,14-15], while the value is about 600 M^{-1} cm^{-1} for a tetranuclear Cu(II) complex [17]. Thus, the ε value for **Complex 1** further supports the presence of two Cu(II) chromophores [16].

Based on all the results discussed above, the proposed structural formula of **Complex 1** is shown in **Figure 4.3**. The proposed structure is consistent with the chemical formula $Cu_2C_{48}H_{82}N_2O_{10}$ (FW = 974.3 g mol^{-1}) as suggested the elemental analyses, and it shows *syn-anti* monodentate bridging $CH_3(CH_2)_{14}COO$ and chelating p-$H_2NC_6H_4COO$ as suggested from FTIR, and square pyramidal geometry at Cu(II) as suggested from UV-vis (local symmetries for the two Cu(II) is C_1).
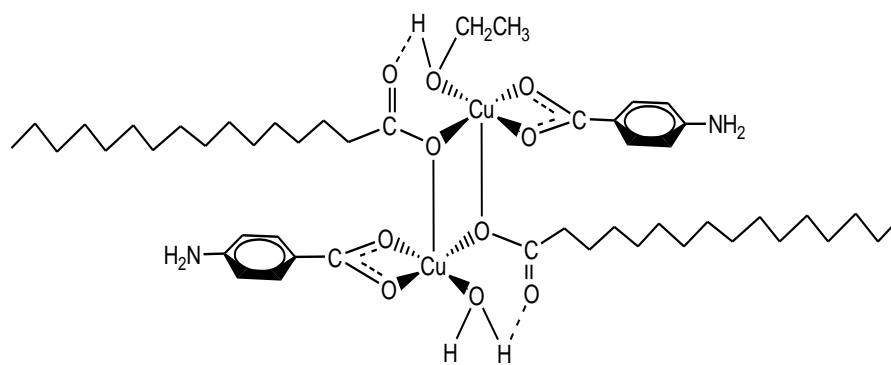
Figure 4.3 *The proposed structural formula of **Complex 1***

The proposed structural formula is further supported by the crystal structure (**Figure 4.4 (a)**) of one of the products formed when **Complex 1** was reacted with 2,2'-bipyridine [18] (**Appendix 3**). The other product was identified as [$Cu_2(p\text{-}H_2NC_6H_4COO)_4$] based on its FTIR spectrum when compared with that of the aromatic "precursor'. The crystal was also obtained from the reaction of [$Cu_2(CH_3(CH_2)_{14}COO)_4$] with 2,2'-bipyridine [24].
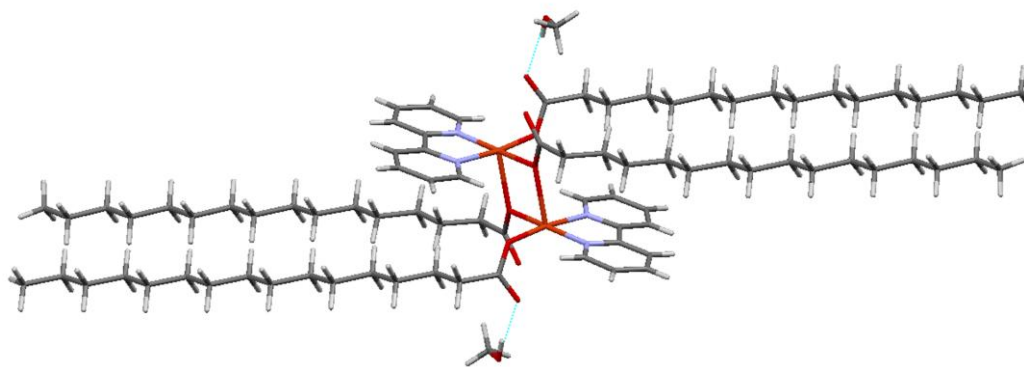
Figure 4.4 (a) *ORTEP diagram for [$Cu_2(CH_3(CH_2)_{14}COO)_2(C_{10}H_8N_2)_2$]*
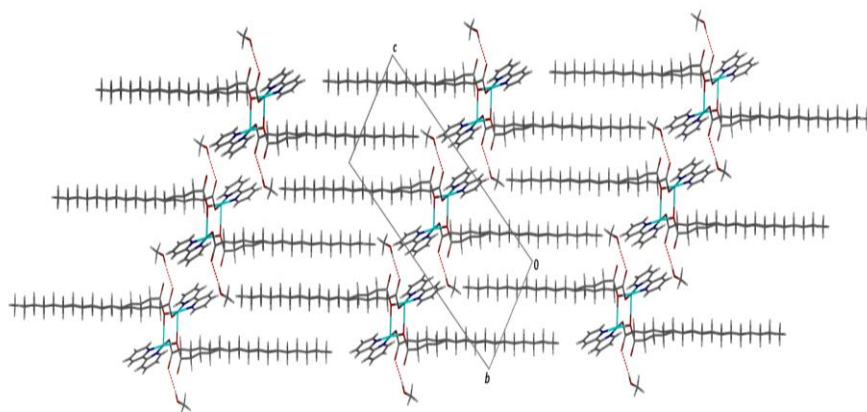
Figure 4.4 (b) *The packing pattern for* $[Cu_2(CH_3(CH_2)_{14}COO)_2(C_{10}H_8N_2)_2]$

The TGA trace (**Figure 4.5**) shows that **Complex 1** is thermally stable up to $256^{o}C$. The initial weight loss from $100^{o}C$ to $117^{o}C$ (6.4%) was due to the evaporation of H_2O and CH_3CH_2OH molecules (expected 6.6%). The total weight loss from $256^{o}C$ to $533^{o}C$ was 76.6% and is assigned to the decomposition of the carboxylate ligands (expected 79.7%) to CO_2 and other volatiles [19]. The amount of residue at above $600^{o}C$ was 17.0%. Assuming that it is CuO [20-22], the estimated formula mass of the complex, calculated using the gravimetric concept, is 936 g mol^{-1} (expected 974 g mol^{-1}). Thus, the results from TGA and elemental analyses are in good agreement.
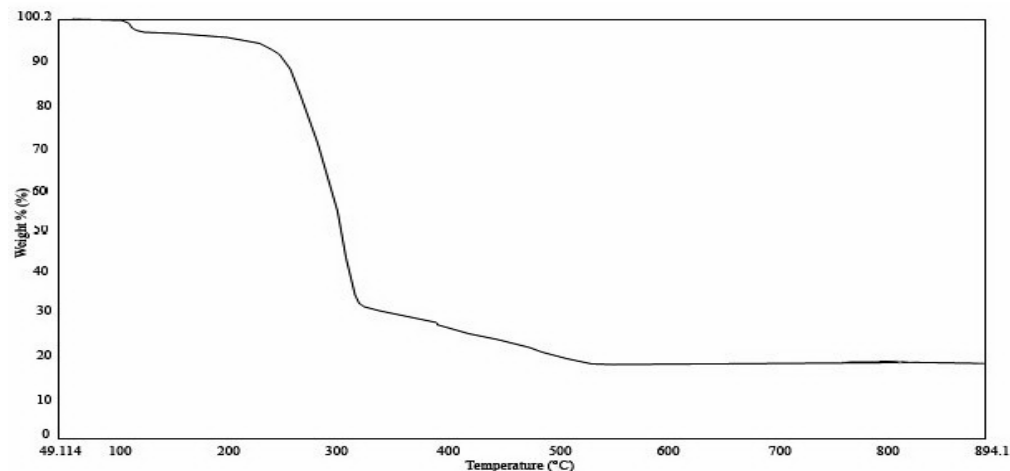
Figure 4.5 *The TGA of **Complex 1***

The DSC of **Complex 1** (**Figure 4.6**) shows two strong overlapping endotherms at 110 $^{\circ}$C and 119 $^{\circ}$C ($\Delta H_{combined}$ = +229 kJ mol^{-1}), assigned to the evaporation of H_2O and CH_3CH_2OH molecules, and melting of the solid, respectively. The high enthalpy for these processes suggests that these molecules were coordinated to Cu(II) and there is strong "intermolecular" interactions due to H-bond between two neighboring p-$H_2NC_6H_4COO$ ligands, and van der Waals forces between the long alkyl chains of $CH_3(CH_2)_{14}COO$ ligand. These endotherms is followed by a very weak endotherm at about 175°C, which is higher than the clearing temperature (133°C). Thus, this endotherm is assigned to the dissociation of the oligomers to dimers, which fits nicely with the darkening of the color observed under POM as a result of geometrical change at Cu(II) from square pyramidal to distorted square planar or tetrahedral. The final broader overlapping endotherms centered at 264°C ($\Delta H_{combined}$ = +121 kJ mol^{-1}), which are above its decomposition temperature (256°C from TGA), are assigned to the breaking of Cu-OOCR$_{(equatorial)}$ bonds, followed by the decomposition of the

carboxylate ligands to volatiles (mainly CO_2) [19]. Thus, the results of DSC and TGA are in good agreement with each other, and consistent with the proposed structural formula.
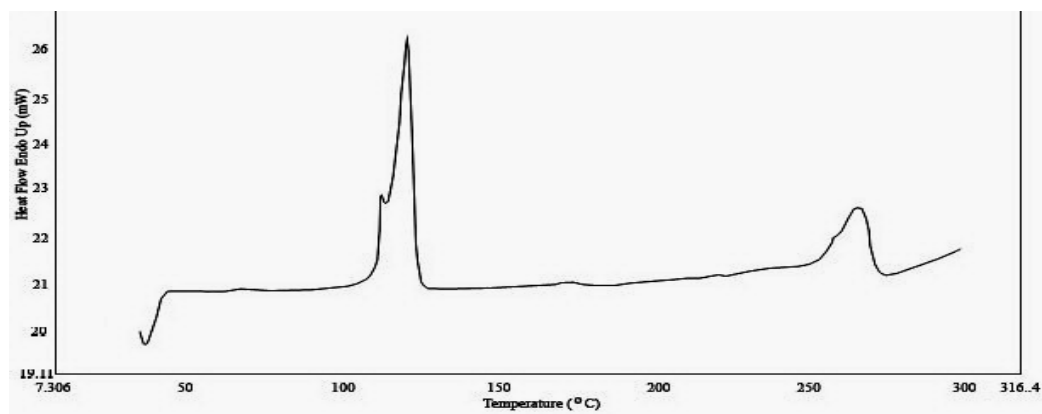
Figure 4.6 *The DSC of* **Complex 1**

Complex 1 when viewed under a plane polarized optical microscope (POM), was observed to melt at $114^{\circ}C$ and cleared to an isotropic liquid at $133^{\circ}C$ (**Figure 4.7(a)**). The color of the liquid darkened on further heating to temperatures below its decomposition temperature. On cooling from the isotropic liquid phase, a smectic C mesophase (SmC) [23] was observed to form at $82^{\circ}C$ (**Figure 4.7(b)**) and remained unchanged on further cooling to room temperature. The observed optical texture is as expected from the rod-like metallomesogen [24], consistent with the proposed structural formula. The change is color on heating is due to loss of H_2O and CH_3CH_2OH, which allows the geometry to change from square pyramidal to square planar, and maximizes the intermolecular interaction to develop the observed optical texture.
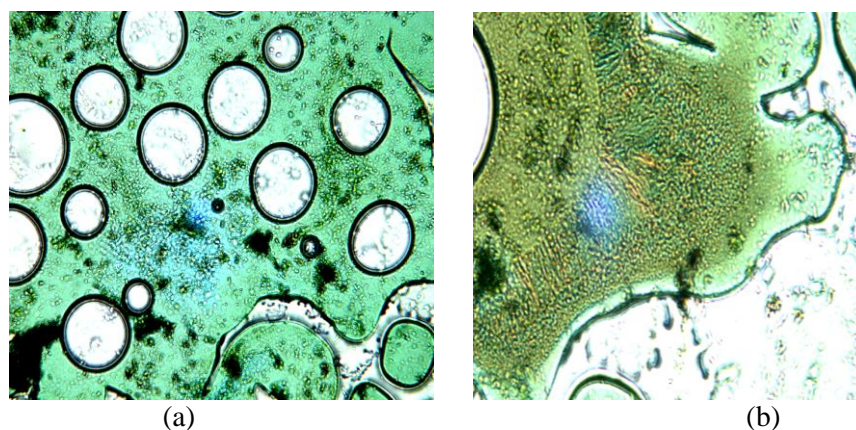
Figure 4.7 *POM of **Complex 1** on (a) heating at 133 ^{o}C (clearing temperature) and (b) cooling at 82 ^{o}C*

The room temperature effective magnetic moment (μ_{eff}) of **Complex 1**, calculated as shown in **Appendix 1**, is 2.79 B.M. This corresponds to the spin-only value for two unpaired electrons (2.83 B.M.). The singlet-triplet separation (-2J), calculated from Bleaney-Bowers equation (**Equation 2.1**), is 20 cm^{-1}. Thus, it may be concluded that there is negligible electronic communication between the two copper(II) centers in the complex. This is in contrast with lower values for most Cu(II) carboxylates reported in the literature. An example is $[Cu_2(CH_3(CH_2)_{14}COO)_4]$, which has the value of 1.45 B.M. at room temperature [25].

However, the negligible electronic communication is consistent with the proposed structural formula (**Figure 4.3**). Similar result was reported for $[Cu(pyrazine-2,3-dicarboxylate)(H_2O)_2].H_2O$, by Konar *et al*. [26]. The authors suggested that the almost negligible coupling between copper(II) ions in their complex was because of the reduction of the magnetic pathway as the basal ligand

was well directed ($d_{x^2-y^2}$ magnetic orbital) but the axial was unfavorably located (d_{z^2} orbital).

The CV of **Complex 1** (**Figure 4.8**), scanned cathodically from 0 V (potential range -1.3 V to +0.8 V), shows overlapping cathodic peaks at -0.47 and at about -0.77 V (shoulder), and overlapping anodic peaks at -0.006 and at about +0.18 V (shoulder).
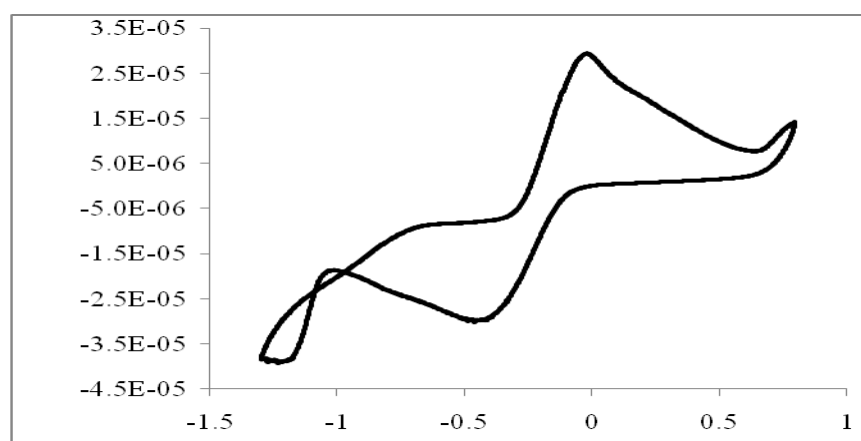
Figure 4.8 *CV of **Complex 1** measured from – 1.3 V to +0.8 V*

The overlapping peaks suggest two Cu(II) centres with negligible electronic interaction, which is consistent with its magnetic properties. Also observed is the nucleation overpotential at -1.1 V, characteristic of a nucleation growth mechanism [27]. The values of the two half-wave potentials, $E_{\frac{1}{2}}^{1}$ and $E_{\frac{1}{2}}^{2}$, are -0.33 V and -0.38 V respectively. These values are in good agreement with that reported for mononuclear [Cu(CH$_3$COO)$_2$(2,2'-bipy)] (-0.37 V) [14]. The redox reactions are summarized below.

$$Cu_2^{II,II} \xrightleftharpoons[\quad]{-0.33\ V} Cu_2^{II,I} \xrightleftharpoons[\quad]{-0.38\ V} Cu_2^{I,I}$$
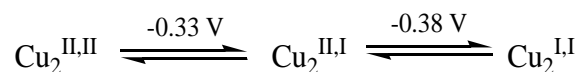
The difference between the half-wave potentials of the two redox processes (ΔE) is a measure of the relative stability of the mixed-valence species ($Cu_2^{II,I}$). This is related to the conproportionation constant, K_{con}, calculated using the relationship, $\log K_{con} = \Delta E/0.0591$. Accordingly, the value of K_{con} for **Complex 1** is 7, which suggests that the mixed-valence species is very unstable, consistent with the negligible exchange interaction between the two Cu(II) centres.

The peaks separation ($E_{pc} - E_{pa}$) are 650 and 764 mV, and the corresponding anodic to cathodic peak currents ratios (i_{pa}/i_{pc}) are 1.2 and 1.0 respectively. From these, it may be suggested that **Complex 1** underwent quasi-reversible, diffusion-controlled electrochemical reactions followed by extensive structural reorganisation. It is noted that there is no large anodic feature on the reverse scan, indicating that the $Cu_2^{I,I}$ species is stabilised towards further reduction or disproportionation to Cu metal, expected at about -0.9 V [14-15].

The electrochemical behaviour of **Complex 1** was further probed by recording its CV in a wider potential range (-1.5 V to +1.0 V; **Figure 4.9**). It is noted that the metal-based redox peaks remained at about the same potentials. However, for the wider potential range, there is an additional cathodic peak at -1.23 V, and two additional anodic peaks at +0.44 and +0.88 V.
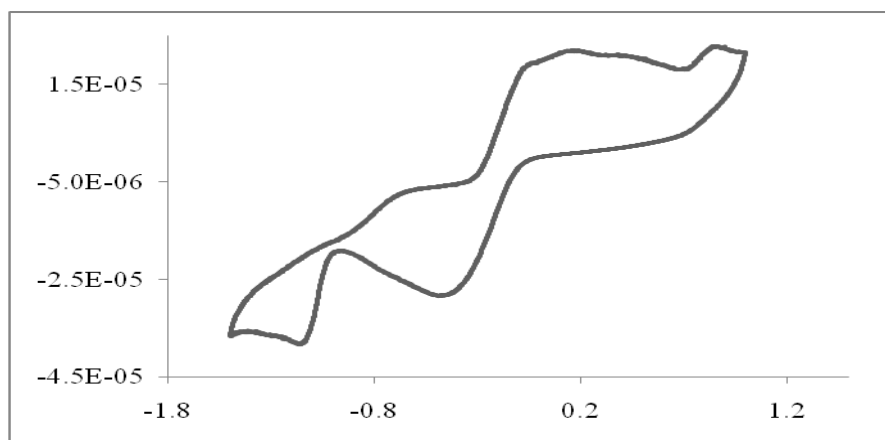
Figure 4.9 *CV of **Complex 1** measured within the potential window of -1.5 V to +1.0V*

In order to correctly assign these new peaks, the CV for its "precursors", $[Cu_2(p\text{-}H_2NC_6H_4COO)_4]$ and $[Cu_2(CH_3(CH_2)_{14}COO)_4]$, were recorded under the same conditions (**Figure 4.10**).
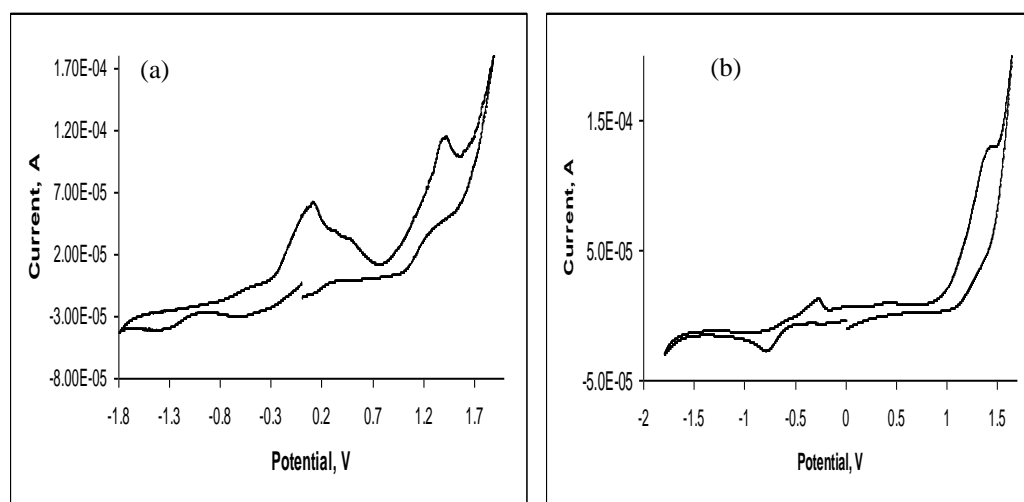
Figure 4.10 *CV of (a) [Cu₂(p-H₂NC₆H₄COO)₄] and (b) [Cu₂(CH₃(CH₂)₁₄COO)₄]*

The CV for the aromatic precursor (**Figure 4.10(a)**) shows two cathodic peaks at -0.62 V and -1.46 V, three overlapping anodic peaks at +0.14 V, +0.35

V, and +0.48 V, and another anodic peak at +1.44 V. In contrast, the CV scan for the aliphatic precursor (**Figure 4.10(b)**) shows a cathodic peak at -0.83 V and two anodic peaks at -0.26 V and +1.45 V. The new cathodic peak at -1.23 V and new anodic peak at +0.44 V for **Complex 1** are in common only with the aromatic precursor (-1.46 V and +0.48 V). Accordingly these peaks are assigned to the reduction and oxidation of p-$H_2NC_6H_4COO$ ligand.

The new anodic peak at +0.88 V for **Complex 1** is in common with both of its "precursors" (but at higher potential of about +1.44 V). Thus, this peak is tentatively assigned to the oxidation of COO fragment of the carboxylate ligands. It is not clear at this stage why this oxidation is more facile for **Complex 1** compared to both of its "precursors".

(ii) Dark green powder

The dark green powder (**Complex 2**) was obtained from the filtrate on complete removal of the solvent. It was soluble in ethanoic acid and pyridine, but insoluble in most other common polar and non-polar organic solvents.

The results of the elemental analyses (48.58% C, 2.64% H, and 8.64% N) are in good agreement with the chemical formula $Cu_2C_{28}H_{28}N_4O_{10}$ (FW = 707 g mol^{-1}; 47.5% C, 3.96% H and 7.9% N). Based on the results of the following analyses, it is proposed that the complex is actually [Cu_2(p-$H_2NC_6H_4COO$)$_4$(H_2O)$_2$], which was one of its precursors.

The FTIR spectrum of the complex (**Figure 4.11(a)**) is similar to that of [Cu_2(p-$H_2NC_6H_4COO$)$_4$] (**Figure 4.11(b)**). It shows the presence of the expected

functional groups based on the proposed structural formula. The ΔCOO values are 138 cm^{-1} (bridging or chelating) and 192 cm^{-1} (*syn-anti* bridging) for the carboxylate ligands [6]. These values suggest a binuclear complex.
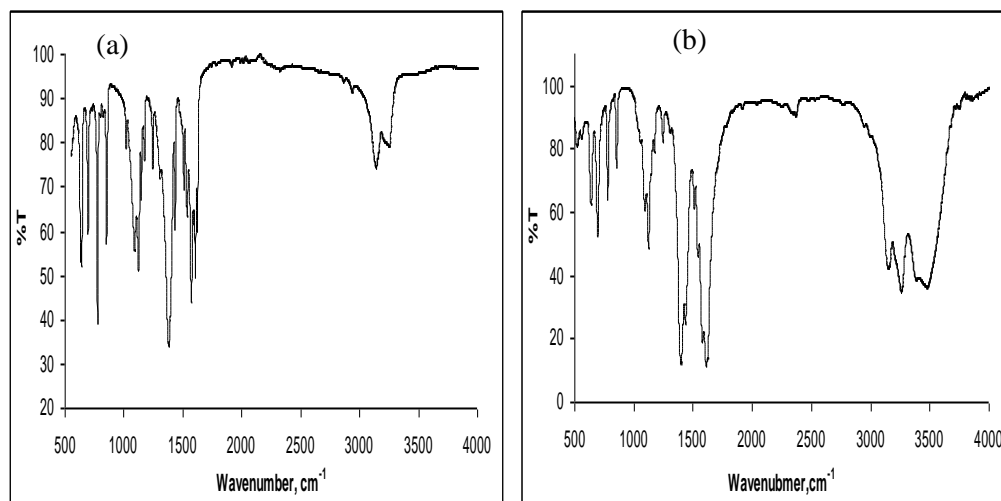
Figure 4.11 *FTIR spectrum of (a)* ***Complex 2*** *and (b) [Cu₂(p-H₂NC₆H₄COO)₄]*

The molar conductivity (Λ_M) of the complex dissolved in DMSO-CH$_3$COOH was 8.0 S cm^2 mol^{-1}. This indicates that the complex is a non-electrolyte and that it did not dissociate into "free" Cu^{2+} and *p*-H$_2$NC$_6$H$_4$COO$^-$ ions in these solvents.

The solid state UV-vis spectrum of the complex **(Figure 4.12(a))** shows two broad *d-d* bands at 617 nm (Band I) and 432 nm (Band II), with absorbance ratio ~ 1:2. The spectrum of the powder dissolved in DMSO-CH$_3$COOH (**Figure 4.12(b)**) shows a broad *d-d* peak at 703 nm (ε = 115 M^{-1}cm^{-1}) for Band I and a weak shoulder at 371 nm (ε = 175 M^{-1}cm^{-1}) for Band II. These observations suggest a change in geometry at the two copper(II) centers from square planar in

the solid state to square pyramidal in solution, due to coordination of the solvent

molecules at the axial positions.
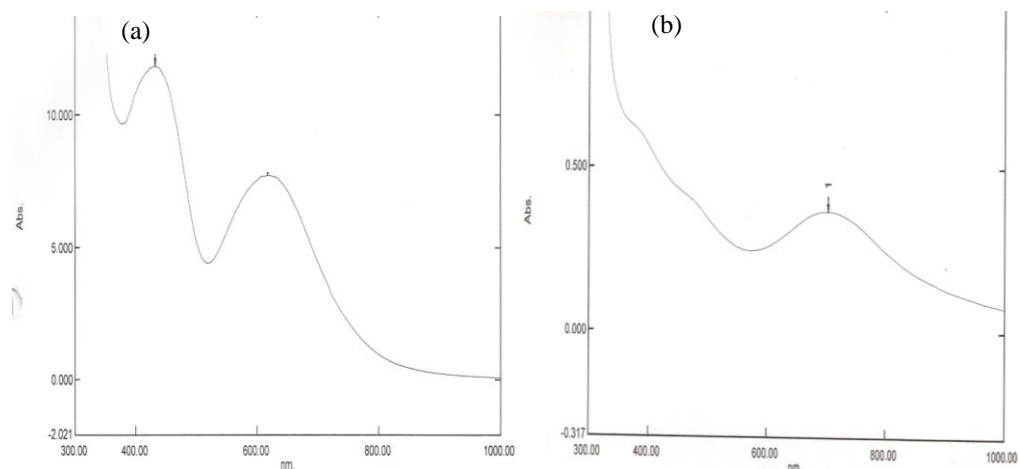
Figure 4.12 *The UV-vis spectra of **Complex 2** as (a) solid (b) solution (DMSO-CH$_3$COOH)*

The TGA trace (**Figure 4.12**) shows that the complex is thermally stable

up to 257°C. The initial weight loss from 128°C to 257°C (3.9 %) is assigned to

the evaporation of two coordinated H$_2$O molecules (expected 5.1%). The total

weight loss from 257°C to 696°C is 73.3% and is assigned to the decomposition

of the carboxylate ligands (expected 76.9%), to CO$_2$ and volatiles compounds

[19].

The DSC (**Figure 4.13**) shows an endotherm at 292°C (ΔH = +158.9 kJ

mol^{-1}) assigned to the decomposition of the carboxylate ligands. Thus, it may be

stated that the DSC and TGA results are in good agreement.
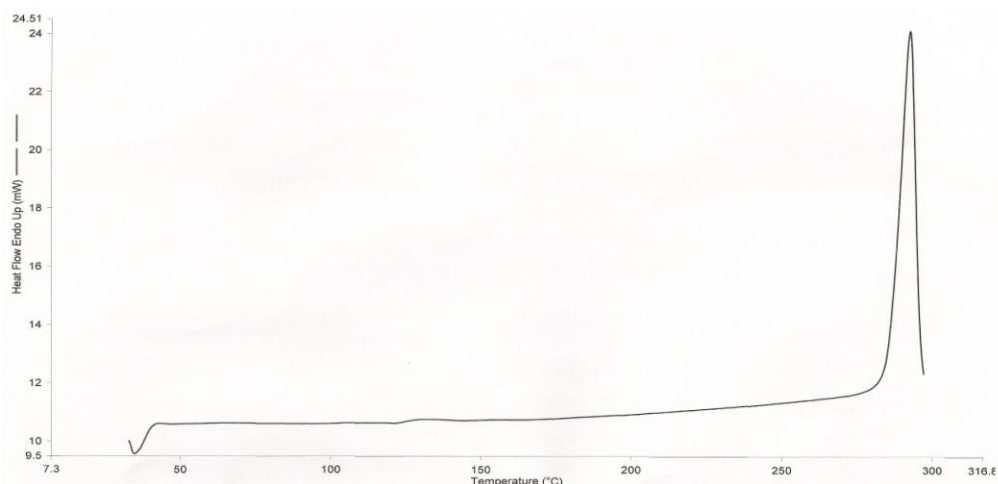
Figure 4.13 *The DSC of Complex 2*

The room temperature effective magnetic moment (μ_{eff}), is 2.35 B.M., while the -2J value is 200 cm^{-1}. The results are as expected for a paddle-wheel dicopper(II) complex. For example, Yilmaz *et al.* [28] found that the binuclear Cu(II) complex of the mixed ligand of diethanolamine (dea) with thiocynate (NCS), [Cu$_2$(μ-dea)$_2$(NCS)$_2$], has the effective magnetic moment of 2.11 B.M. The complex showed a high-spin configuration as a result of the doubly oxygen-bridged dimeric structure that leads to the subnormal magnetic moment due to the super-exchange interaction.

The CV of the complex, scanned cathodically from 0 V in the potential range of -1.3 V to +1.5 V, shows cathodic peaks at similar voltammogram as observed for [Cu$_2$(*p*-H$_2$NC$_6$H$_4$COO)$_4$] (**Figure 4.14; Table 4.2**).
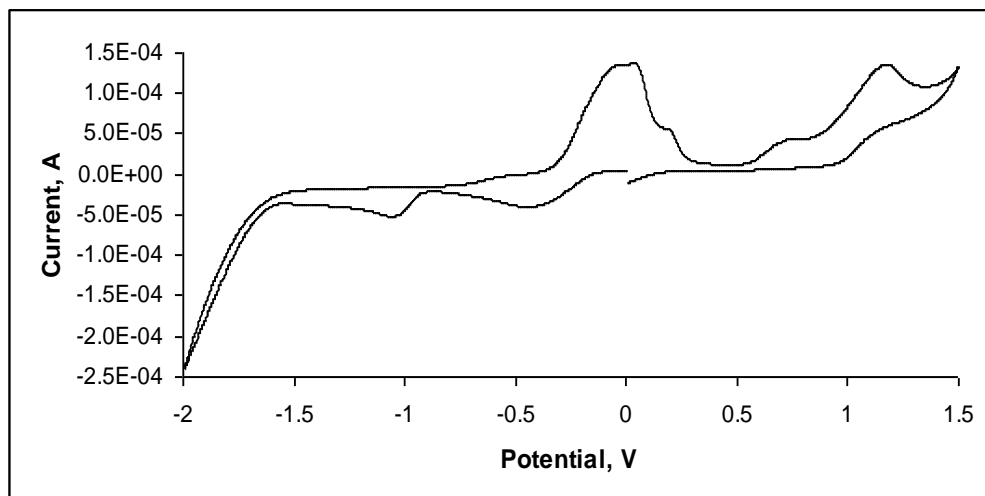
Figure 4.14 *CV of **Complex 2** measured from -2.0 V to +1.5 V*

Table 4.2 *CV data for **Complex 2** and [Cu$_2$(p-H$_2$NC$_6$H$_4$COO)$_4$]*

Complex	Cathodic peak (V)		Anodic peak (V)			
Complex 2	-0.60	-1.45	+0.15	+0.37	+0.53	+1.45
[Cu$_2$(*p*-H$_2$NC$_6$H$_4$COO)$_4$]	-0.62	-1.46	+0.14	+0.35	+0.48	+1.44

To summarize, the one-pot reaction using Cu(NO$_3$)$_2$ was successful in obtaining [Cu$_2$(*p*-H$_2$NC$_6$H$_4$COO)$_2$(CH$_3$(CH$_2$)$_{14}$COO)$_2$(H$_2$O)(CH$_3$CH$_2$OH)] in moderate yield (34.2%). The complex was thermally stable, metallomesogenic, magnetic and redox active. The reaction also formed [Cu$_2$(*p*-H$_2$NC$_6$H$_4$COO)$_4$(H$_2$O)$_2$], which is one of the precursor of the intended complex.

4.2.2 Reaction between Cu(CH₃COO)₂, p-H₂NC₆H₄COOH and CH₃(CH₂)₁₄COOH

4.2.2 Reaction between $Cu(CH_3COO)_2$, $p\text{-}H_2NC_6H_4COOH$ and $CH_3(CH_2)_{14}COOH$

Two products were isolated from the one-pot reaction using equimolar ratio of [Cu(CH₃COO)₂], p-H₂NC₆H₄COOH and CH₃(CH₂)₁₄COOH: a dark green powder (31.2%) and a pale blue powder (61.1%).

(i) Dark green powder

The dark green powder (**Complex 3**) was the residue isolated from the hot reaction mixture. Based on the following evidence, it is proposed to have the chemical formula $Cu_2C_{37}H_{54}N_4O_9$ or [Cu₂(p-H₂NC₆H₄COO)₃(CH₃(CH₂)₁₄COO)(H₂O)(NH₃)]. The results of the elemental analyses (52.23% C, 5.11% H, 6.48% N) are in good agreement with the values calculated for $Cu_2C_{37}H_{54}N_4O_9$ (FW = 825.1 g mol⁻¹; 53.8% C, 6.54% H and 6.78% N).

The FTIR (**Figure 4.15**) spectrum shows the presence of the expected functional groups based on the proposed structural formula. The ΔCOO value is 106 cm⁻¹ and 194 cm⁻¹, suggesting chelating and bridging (monoatomic, *syn-anti*) carboxylate ligands respectively [6], and thus a binuclear complex.
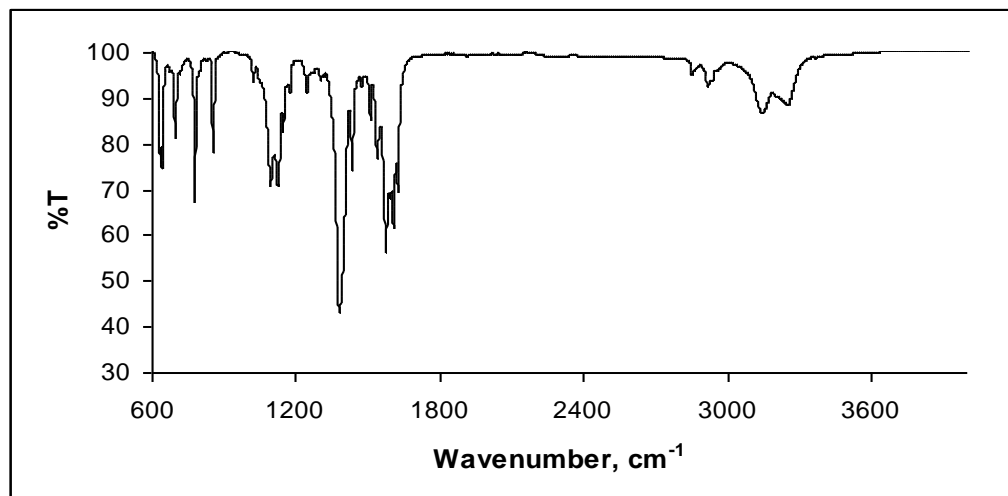
Figure 4.15 *FTIR spectrum of* **Complex 3**

The molar conductivity (Λ_M) of the complex, dissolved in DMSO-CH$_3$COOH, was 9.7 S cm^2 mol^{-1}. This indicates that it is a non-electrolyte, and that it did not dissociate to "free" Cu^{2+} and p-H$_2$NC$_6$H$_4$COO$^-$ ions in this solvents, as was found for **Complex 1** and **Complex 2**.

The solid state UV-vis spectrum of **Complex 3** (**Figure 4.16(a)**) shows two broad *d-d* bands at 624 nm (Band I) and 442 nm (Band II), with absorbance ratio of about 1:1. Thus, its geometry at Cu(II) is square pyramidal. The spectrum of the complex dissolved in DMSO-CH$_3$COOH (**Figure 4.16(b)**) shows a broad *d-d* peak at 713 nm ($\varepsilon = 388$ M^{-1}cm^{-1}) for Band I and a weak shoulder at about 400 nm ($\varepsilon = 291$ M^{-1} cm^{-1}) for Band II. Thus, the geometry at Cu(II) remained unchanged in these solvents.
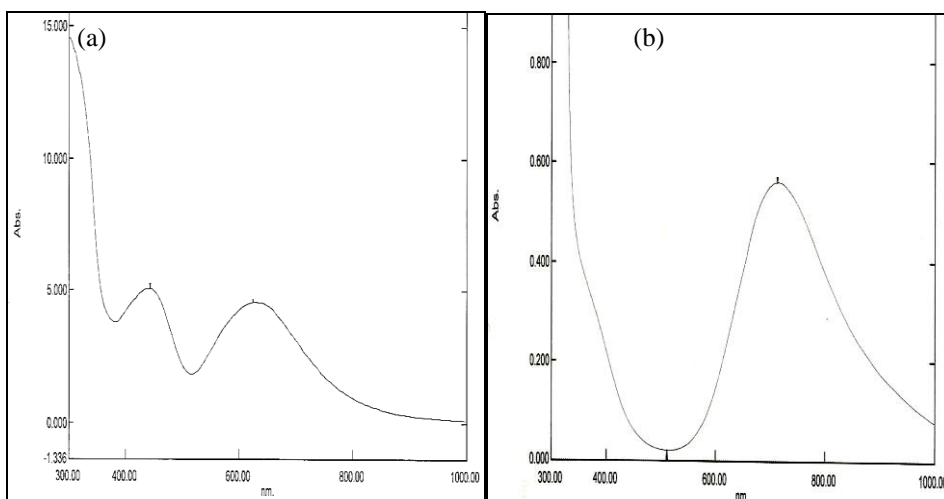
Figure 4.16 *The UV-vis spectra of **Complex 3** as (a) solid (b) solution (DMSO-CH₃COOH)*

Based on the results discussed above, the proposed structural formula of **Complex 3** is shown in **Figure 4.17**. The proposed structure is consistent with the chemical formula $Cu_2C_{37}H_{54}N_4O_9$ (FW = 825.1 g mol^{-1}) as suggested the elemental analyses, *syn-anti* monodentate bridging $CH_3(CH_2)_{14}COO$ and chelating p-$H_2NC_6H_4COO$ as suggested from FTIR, and square pyramidal geometry at Cu(II) as suggested from UV-vis (local symmetries for the two Cu(II) are C_{2v} and C_1).
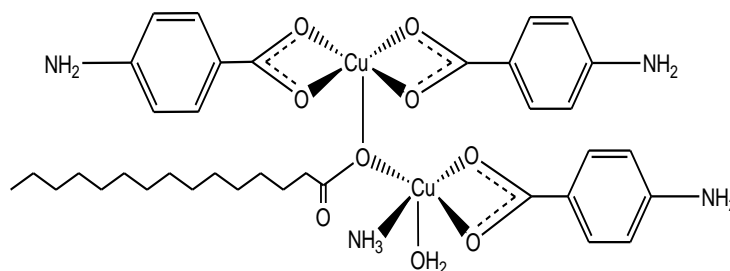
Figure 4.17 *Proposed structural formula of **Complex 3***

The proposed structural formula also explains the shift to lower energy for Band I and to higher energy for Band II when the solid was dissolved in DMSO-CH_3COOH (**Figure 4.18**).

(a)   (b)
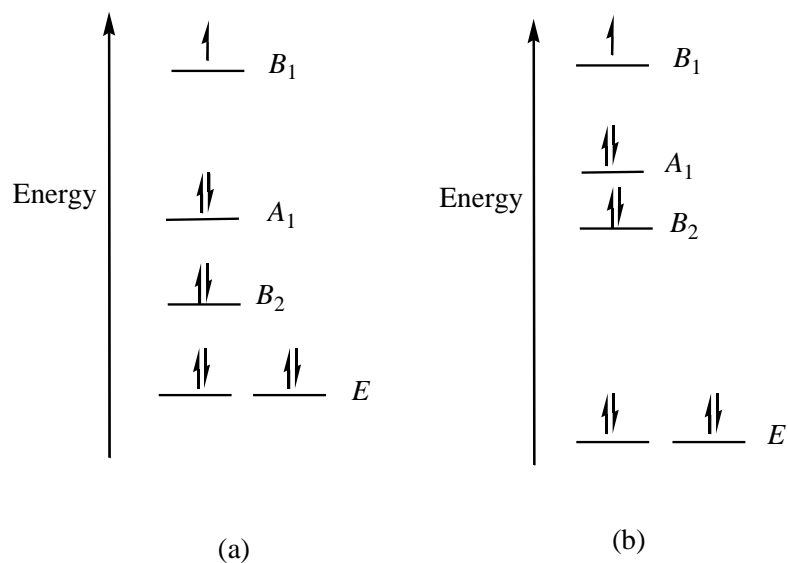
Figure 4.18 The energy level diagram (not to scale) for Cu(II) : (a) square pyramidal geometry in the solid state; and (b) elongated octahedral geometry in solution

In the solid state (**Figure 4.16 (a)**), the electronic transitions are assigned based on the C_{4v} point group, as follows: $B_2 \rightarrow B_1$ (Band I; 624 nm) and $E \rightarrow B_1$ (Band II; 442 nm). The $A_1 \rightarrow B_1$ transition appears as a shoulder at the low energy end of Band I.

In the solution (**Figure 4.16 (b)**), the ligand NH_3 reacted with CH_3COOH in the solvent, thus temporarily freeing one of the equatorial positions. As a result, the monoatomic $CH_3(CH_2)_{14}COO$ that initially *syn,anti*-bridged the two Cu(II) rearranged to chelate one Cu(II), forming two mononuclear complexes with

DMSO molecules coordinated at the axial positions elongated octahedral Cu(II) centres.
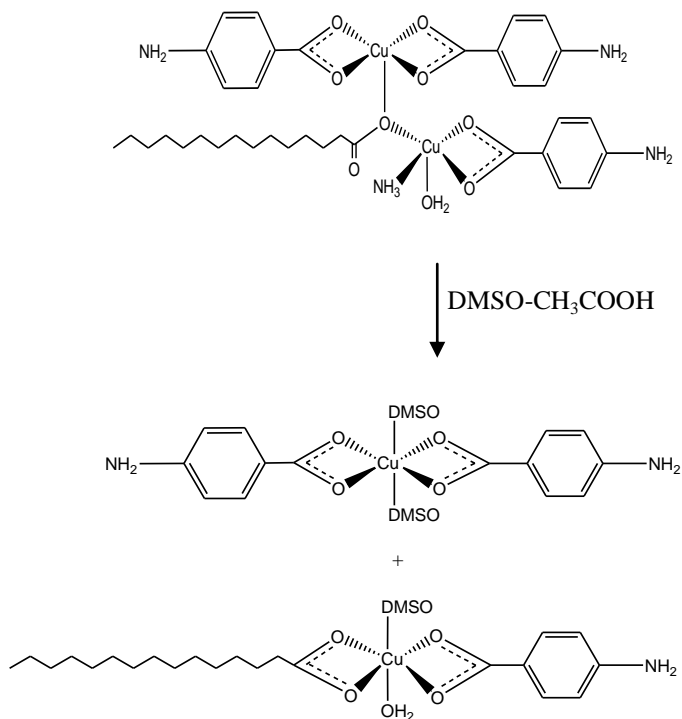
The effect of the above reaction is to produce a highly symmetrical mononuclear complex (D_{2h} symmetry) and a highly unsymmetrical mononuclear complex (C_1 symmetry). Under octahedral geometry, the electronic transition corresponding to Band I decrease in energy. The d orbitals of Cu(II) that are most strongly affected by the distortion are the d_{xy} (B_2), and d_{xz}, d_{yz} (E). The energy of the d_{xy} orbital is expected to decrease (increase in stability) as the ligands move away from it, while the energy of the (d_{xz}, d_{yz}) orbitals are expected to increase (decrease in stability) as the ligands move nearer to it. Thus, the assignments are: $E \rightarrow B_1$ (Band I; 713 nm) and $B_2 \rightarrow B_1$ (Band II; ~400 nm).

The geometry of both Cu(II) centres are distorted out of the x,y plane towards the z axis. The effects are to increase the energy of the xy orbital (B_2) and decrease the energy of the $x^2\text{-}y^2$ orbital.

The TGA thermogram (**Figure 4.19**) shows that the complex is thermally stable up to 222°C. The initial weight loss from 100°C to 135°C (5.0%) is assigned to the evaporation of H_2O and NH_3 molecules (expected 4.5%). The total weight loss from 222°C to 500°C is 79.6% and is assigned to the decomposition of the carboxylate ligands (expected 80.3%) to carbon dioxide and other volatiles.
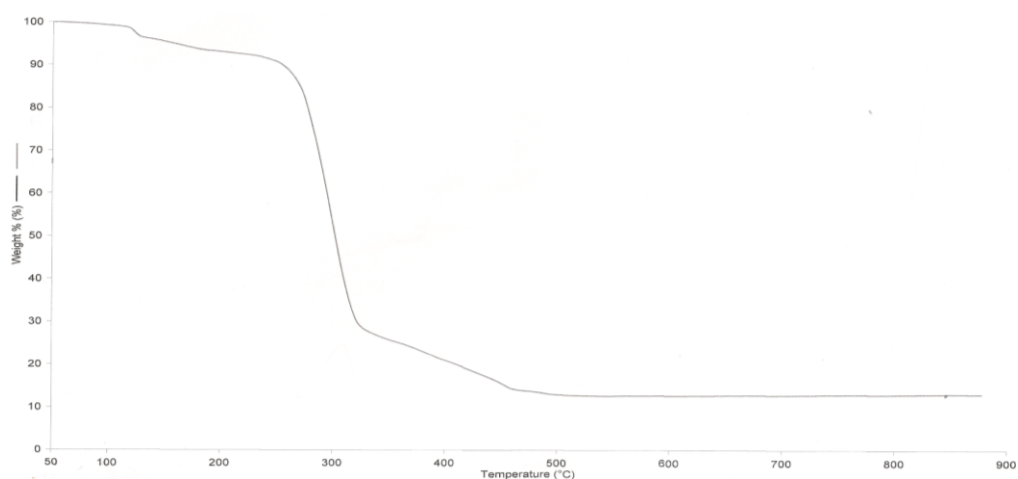
Figure 4.19 *TGA thermogram of **Complex 3***

The DSC (**Figure 4.20**) shows two overlapping endotherms at 116°C (combined $\Delta H = +18.6$ kJmol^{-1}) assigned to the evaporation of NH_3 and H_2O molecules, and another strong endotherm at 280°C ($\Delta H = +110.6$ kJmol^{-1}) assigned to the decomposition of the carboxylate ligands. Thus, it may be stated that the DSC and TGA results are in good agreement with each other.
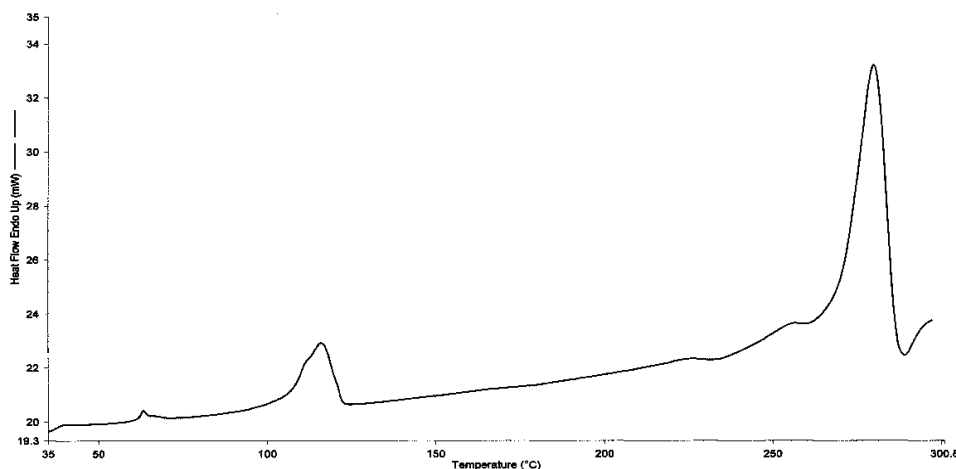
Figure 4.20 *DSC scan of* ***Complex 3***

The room temperature effective magnetic moment (μ_{eff}), calculated as previously done, is 2.84 B.M. The -2J value is -109 cm^{-1}.Thus, it may be concluded that there exists a ferromagnetic interaction between the two copper(II) centre in the complex, in contrast to **Complex 1**. This further supports the proposed structure for the complex.

The cyclic voltammetry, scanned cathodically from 0 V in the potential range -2.0 V to +1.5 V (**Figure 4.21**), shows two reduction peaks at -0.40 V and -1.1 V, three overlapping oxidation peaks at –0.08 V, +0.03 V and +0.20 V, and another oxidation peak at +1.1 V The value of ΔE are 370 mV and 1240 mV, and the corresponding ratios of the anodic and cathodic peak currents (I_{pa}/I_{pc}) are 3.2 and 1.9. From these, it may be suggested the complex underwent a quasi-reversible electrochemical reaction followed by an extensive structural reorganization (EC mechanism), and that the mixed valence [Cu(II)Cu(I)] and homovalence [Cu(I)Cu(I)] complexes were chemically unstable.
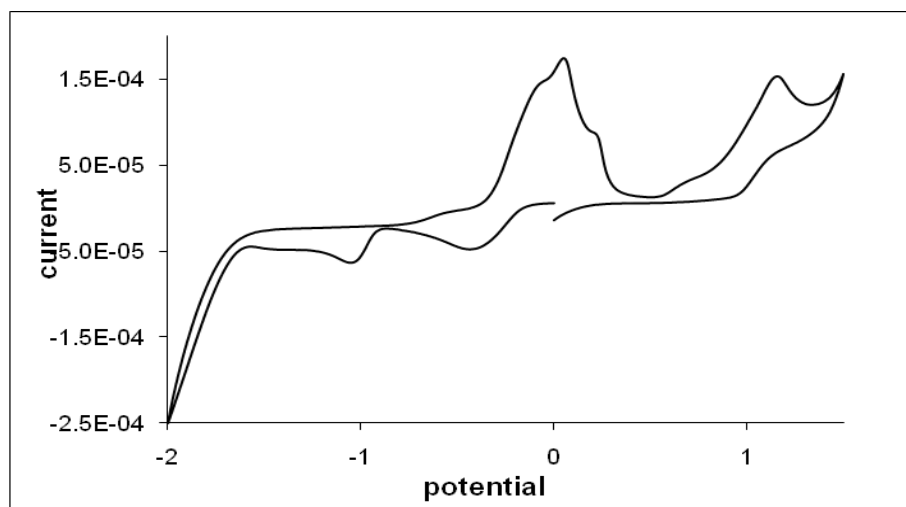
Figure 4.21 *CV scanned of* ***Complex 3***

The presence of two reduction peaks is consistent with a dicopper(II) complex with two Cu(II) atoms in a different environment, labeled as Cu^A and Cu^B in **Figure 4.22**. The geometry at Cu^A is more distorted and thus it is easier to be reduced compared to the less distorted Cu^B.
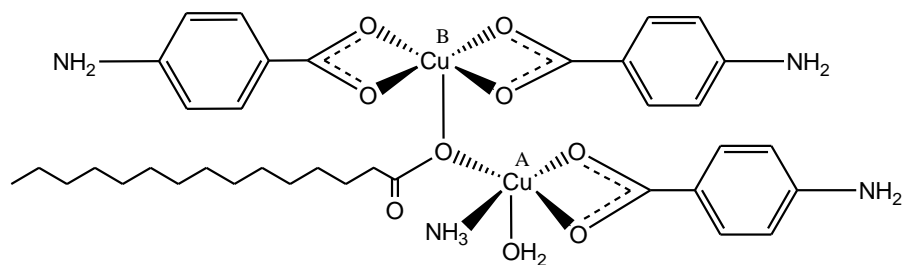
Figure 4.22 *The proposed structural formula of* ***Complex 3*** *with the two Cu(II) atoms labeled to show the different environment*

The fully reduced [Cu(I)^{A}Cu(I)^B] seemed to partially disproportionate to mononuclear Cu(II) and Cu(O). Hence, there were two species present when the

mixture was reoxidised, specifically $[Cu(I)^ACu(I)^B]$ and Cu(0). The redox reactions are summarized below.

$$[Cu(II)^ACu(II)^B] \underset{+0.03V}{\overset{-0.40V}{\rightleftharpoons}} [Cu(I)^ACu(II)^B] \underset{+0.20V}{\overset{-1.04V}{\rightleftharpoons}} [Cu(I)^ACu(I)^B]$$

$$[Cu(I)^ACu(I)^B] \xrightarrow{\text{disproportionation}} Cu(II) + Cu(0)$$

$$Cu(0) \xrightarrow{-0.08 \text{ V}} Cu(I) \xrightarrow{+1.1 \text{ V}} Cu(II)$$
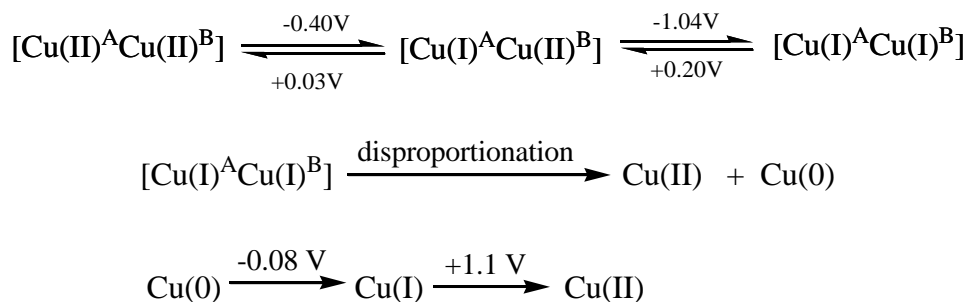
Similar redox behavior was also reported by Perlepes et al. [6] for $[Cu_2(CH_3COO)_4(2,2'\text{-bipy})_2].2H_2O$, in which the CH_3COO^- ligand was also bonded to the two Cu(II) atoms in the *syn-anti* bridging mode as proposed for **Complex 3.**

(ii) Pale blue powder

The pale blue powder that deposited out of the filtrate after standing for 24 hours, based on the instrumental analyses, is actually **Complex 1** ($[Cu_2(p\text{-}H_2NC_6H_4COO)_2(CH_3(CH_2)_{14}COO)_2(H_2O)(CH_3CH_2OH)]$.

The results of the elemental analyses (59.93% C, 11.28% H and 2.19% N) are in good agreement with those calculated for $Cu_2C_{48}H_{82}N_2O_{10}$ (MW = 974.3 gmol^{-1}; 59.17% C, 8.48% H and 2.88% N). The FTIR spectrum (**Figure 4.23)** and UV-vis spectra in both the solid state and in solution (**Figure 4.24**) are also similar to that of **Complex 1** (**Section 4.2(a)(i)**).
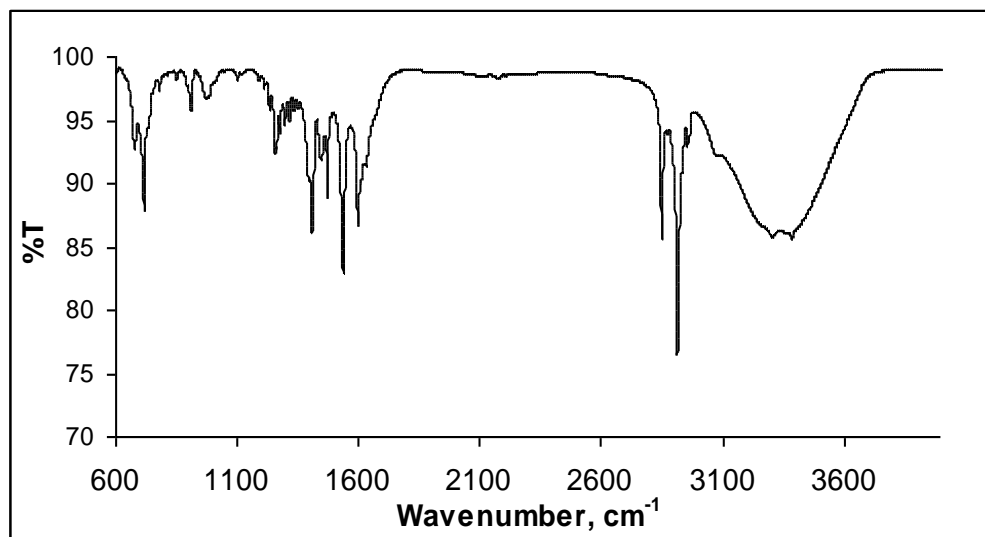
Figure 4.25 *FTIR spectrum of pale blue powder*
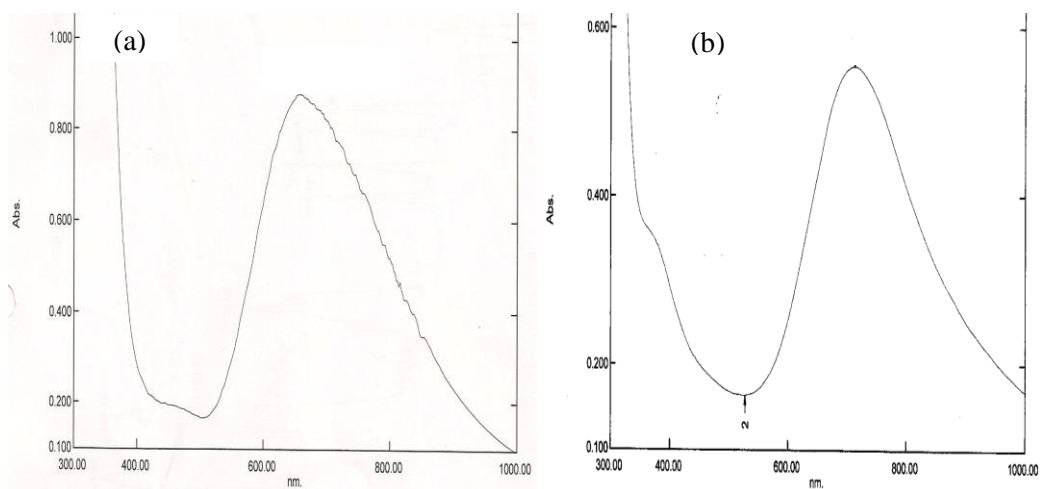
Figure 4.25 *UV-vis spectra of the pale blue powder as: (a) solid (b) solution (DMSO-CH$_3$COOH)*

4.2.3 Reaction between CuSO$_4$, p-H$_2$NC$_6$H$_4$COOH and CH$_3$(CH$_2$)$_{14}$COOH

The reaction using equimolar ratio of CuSO$_4$, p-H$_2$NC$_6$H$_4$COOH and CH$_3$(CH$_2$)$_{14}$COOH gave only one product, a pale blue powder, which deposited out from the hot reaction mixture. The same pale blue powder was also obtained

on complete removal of the solvent from the filtrate. The total yield of the product is 54.7%.

Based on the instrumental analyses, the complex is actually **Complex 1** ($[Cu_2(p\text{-}H_2NC_6H_4COO)_2(CH_3(CH_2)_{14}COO)_2(H_2O)(CH_3CH_2OH)]$). The results of the elemental analyses (58.72% C, 10.98% H and 1.96% N) are in good agreement with the chemical formula $Cu_2C_{48}H_{82}N_2O_{10}$ (FW = 974.3 g mol^{-1}; 59.17% C, 8.48% H and 2.88% N).

The FTIR spectrum (**Figure 4.26) and** UV-vis spectra in both the solid state and in solution (**Figure 4.27**) are also similar to that of **Complex 1** (**Section 4.2(a)(i)**).

.
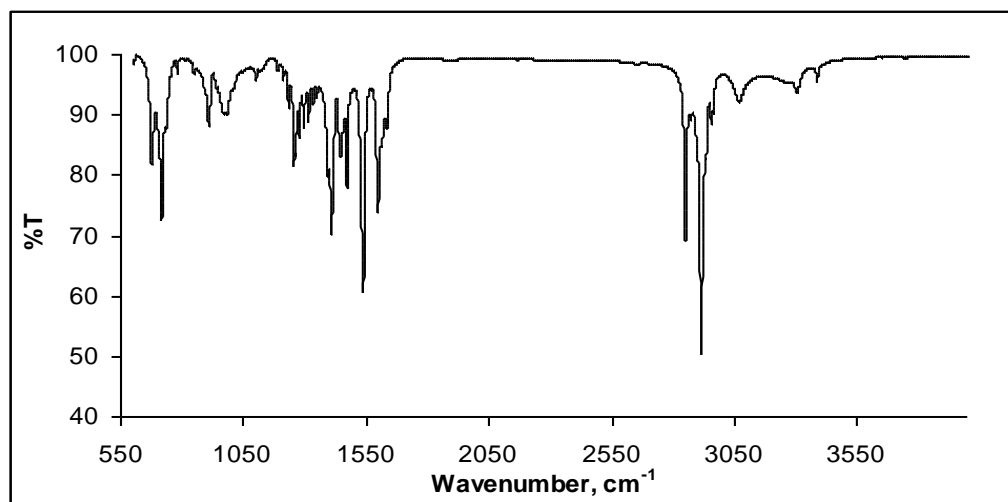
Figure 4.26 *FTIR spectrum of the pale blue powder*
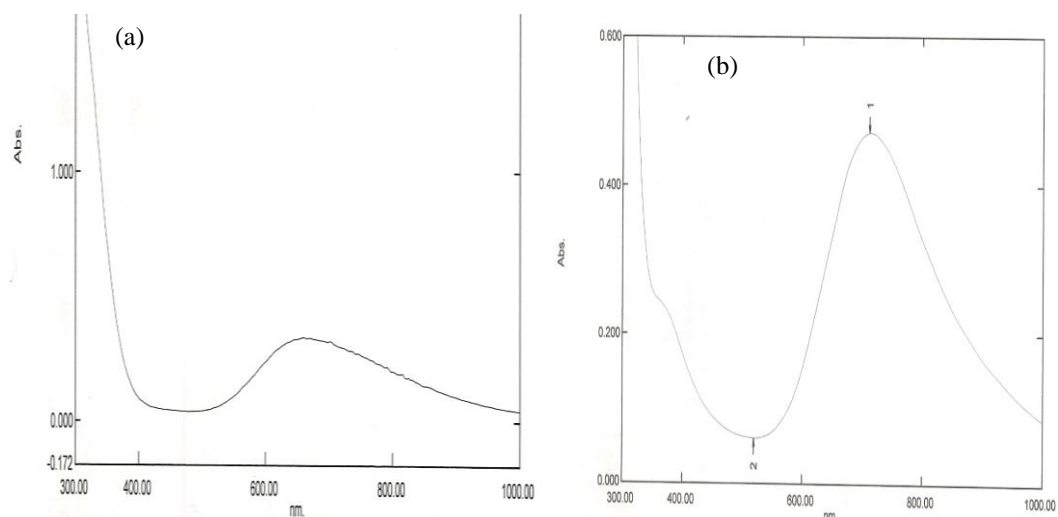
Figure 4.27 *The UV spectra of the pale blue powder as: (a) solid and (b) solution in (DMSO-CH3COOH)*

4.2.4 Reaction between $CuCl_2$, p-$H_2NC_6H_4COOH$ and $CH_3(CH_2)_{14}COOH$

Two products were isolated from the reaction involving equimolar ratio of $CuCl_2$, p-$H_2NC_6H_4COOH$ and $CH_3(CH_2)_{14}COOH$: (a) a pale green powder (34.6%) and (b) a dark green powder (12.9%).

(i) Pale green powder

The pale green powder **(Complex 4)** was a residue from hot reaction mixture. It was soluble in the same solvents as **Complex 1**. The results of the elemental analyses (32.58% C, 3.94% H, and 7.74% N) are in good agreement with the chemical formula $Cu_2C_{21}H_{34}N_4O_{11}Cl_4$ (FW = 787.5 g mol^{-1}; 32.02% C, 4.35% H and 7.12% N). Based on the results of the following analyses, the proposed structural formula for **Complex 4** is [$Cu_2(p$-$H_3NC_6H_4COO)_3Cl(H_2O)_2$]$Cl_3.NH_3.3H_2O$.

The FTIR spectrum (**Figure 4.28**) shows the presence of the expected functional groups as discussed previously. The ΔCOO values are 195 cm^{-1} and 125 cm^{-1} suggesting monodentate *syn-anti* bridging and chelating/bridging carboxylate ligands, respectively. From these, a binuclear complex may be inferred.
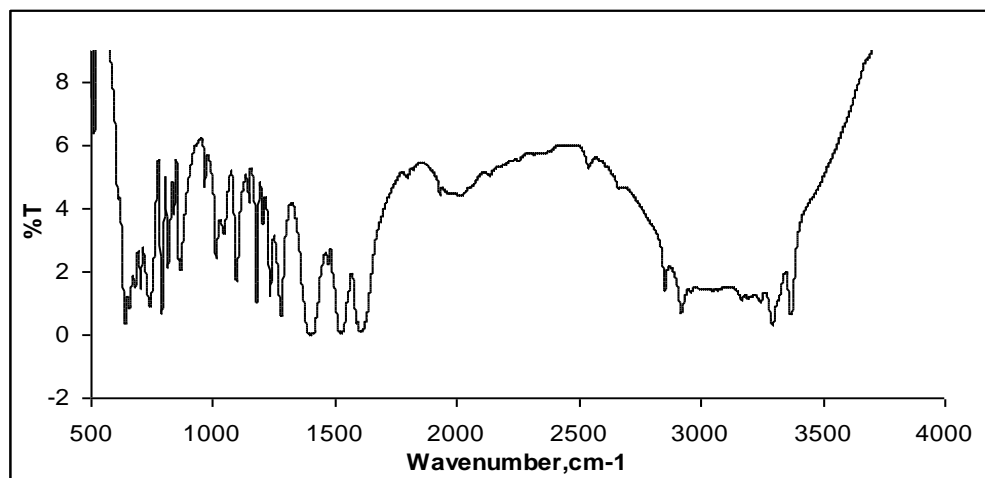
Figure 4.28 *FTIR spectrum of* ***Complex 4***

The value of Λ_M of **Complex 4** in DMSO-CH$_3$COOH was 76 S cm^2 mol^{-1}. The high value means that the complex is a 1:1 electrolyte in solution. This is in contrast with previous complexes, which were non-electrolytes in these solvents.

The solid state UV-vis spectrum of **Complex 4** (**Figure 4.29(a)**) shows a broad *d-d* band at 702 nm (Band I). The spectrum of the powder dissolved in DMSO-CH$_3$COOH (**Figure 4.29(b)**) shows a broad *d-d* peak at 713 nm (ε = 617 M^{-1} cm^{-1}) for Band I and a weak shoulder at 389 nm (ε = 422 M^{-1} cm^{-1}) for Band II. These observations suggest a binuclear complex with square pyramidal geometry at the two copper(II) centres in the solid state, and the geometry is maintained in these solvents.
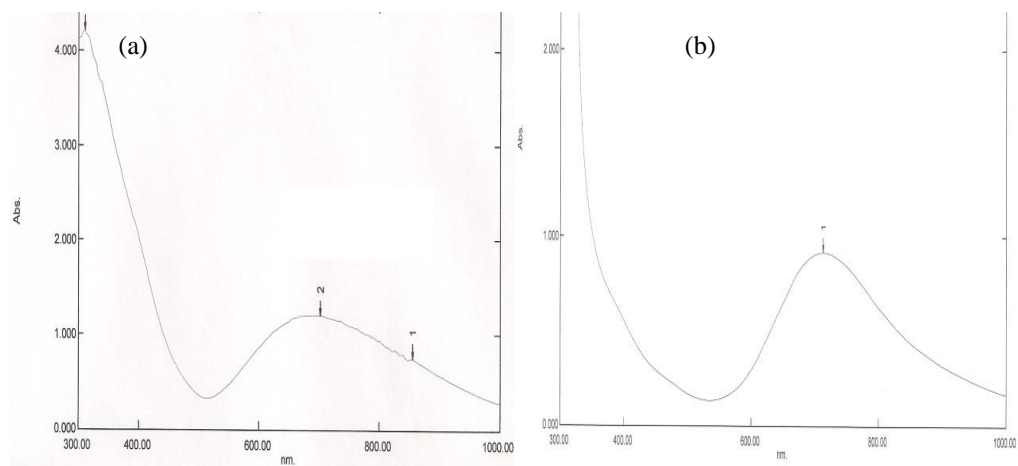
Figure 4.29 *The UV-vis spectra of the (a) solid (b) solution (DMSO-CH₃COOH)*

Based on all the results discussed above, the proposed structural formula of the **Complex 4** is [Cu₂(*p*-H₃NC₆H₄COO)₃Cl(H₂O)₂]Cl₃.NH₃.3H₂O (**Figure 4.30**). The proposed structure is consistent with the chemical formula Cu₂C₂₁H₃₄N₄O₁₁Cl₄ (FW = 788.13 g mol⁻¹) as suggested the elemental analyses, monoatomic *syn-anti* bridging and chelating *p*-H₃NC₆H₄COO as suggested from FTIR, and square pyramidal geometry at Cu(II) as suggested from UV-vis.
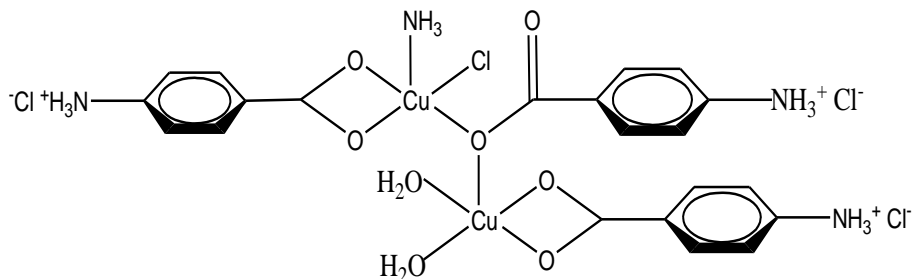
Figure 4.30 *Proposed structural formula of* **Complex 4** *(H₂O solvates are not shown)*

The TGA trace (**Figure 4.31**) shows that **Complex 4** is thermally stable up to 210°C. The initial weight loss of 3.0% at about 75°C is assigned to loss of axially coordinated NH_3 molecule (expected, 2.2%). The next weight loss of 12.8% at 156°C is assigned to the evaporation of five H_2O molecules (expected, 11.4%). The total weight loss of 73.6 % from 210°C to 670°C is assigned to the decomposition of p-$H_2NC_6H_4COO$ ligands and evaporation of HCl molecules (expected, 70.2 %) to carbon dioxide and other volatiles.

The amount of residue above 670°C is 10.6% (expected, 20.2% if CuO, and 18.1% if Cu_2O). This seems to suggest that the complex formed volatile copper(II) complexes above this temperature.
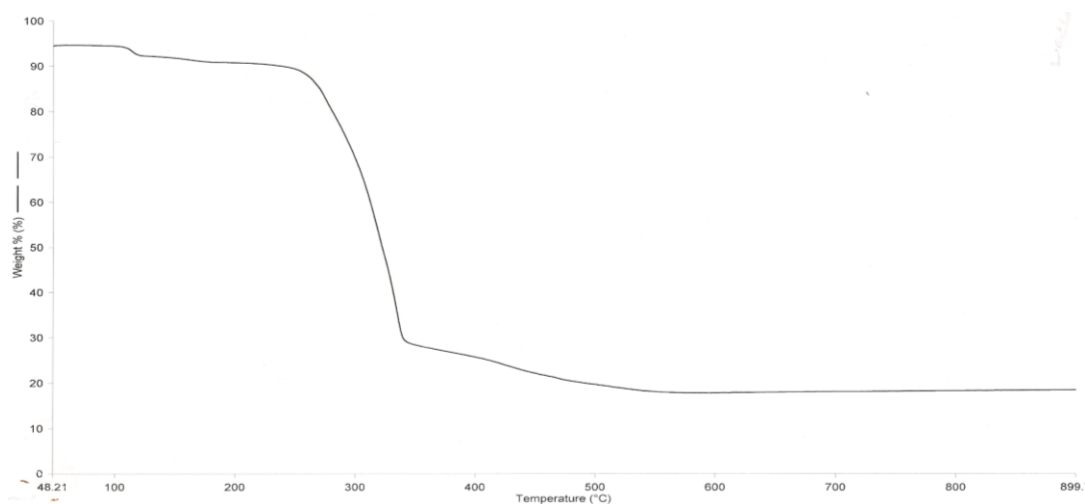
Figure 4.31 TGA *of* Complex 4

The DSC of **Complex 4** (**Figure 4.32**) shows a strong endotherm at 166°C ($\Delta H = +169.9$ kJ mol^{-1}) and a weak endotherm at 269°C ($\Delta H = +9.1$ kJmol^{-1}). The first endotherm, which occurred below its decomposition temperature (210°C), is assigned to the evaporation of coordinated H_2O molecules. The second

endotherm, which occurred above its decomposition temperature, is assigned to loss of HCl from the aromatic ligands. Thus, it may be stated that the DSC and TGA results are in good agreement with each other.
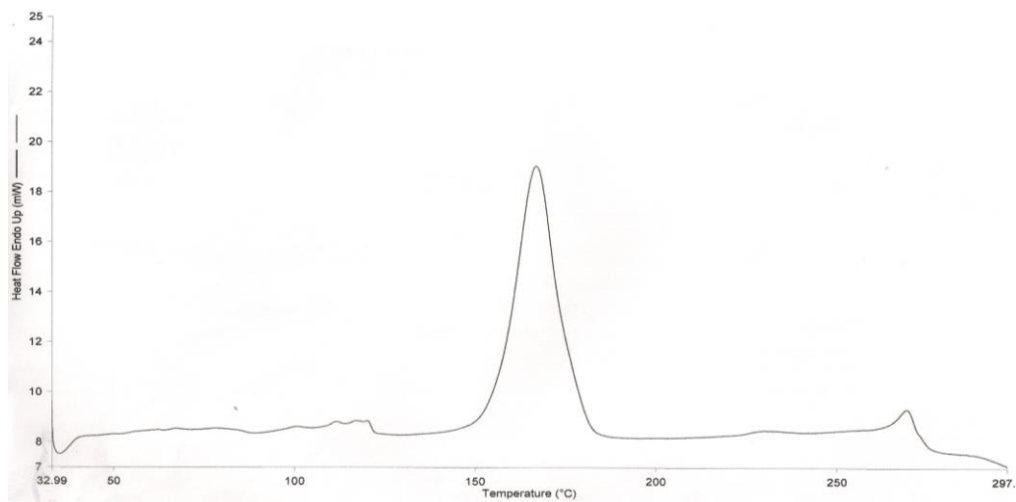
Figure 4.32 DSC *of Complex 4*

The OPM micrograph was not recorded as this complex is not expected to be metallomesogen.

The values of μ_{eff} and -2J for **Complex 4** are 3.72 B.M. and 37.8 cm^{-1} respectively. These indicate ferromagnetic interaction between the two Cu(II) centres, in contrast to antiferromagnetic interaction for **Complex 1**. It is noted that **Complex 4** is ionic while **Complex 1** is neutral. Thus, the difference in the magnetic properties may be due to better alignment in the ionic complex as a result of dipolar interaction between the dimers.

The CV (**Figure 4.33**) was scanned cathodically from 0 V in the potential range of -2.0 V to +2.0 V shows two broads cathodic peaks at about -0.40 V and -

1.18 V, and two overlapping anodic peaks at about +0.11 V and +0.31 V and another anodic peak at around +1.13 V.
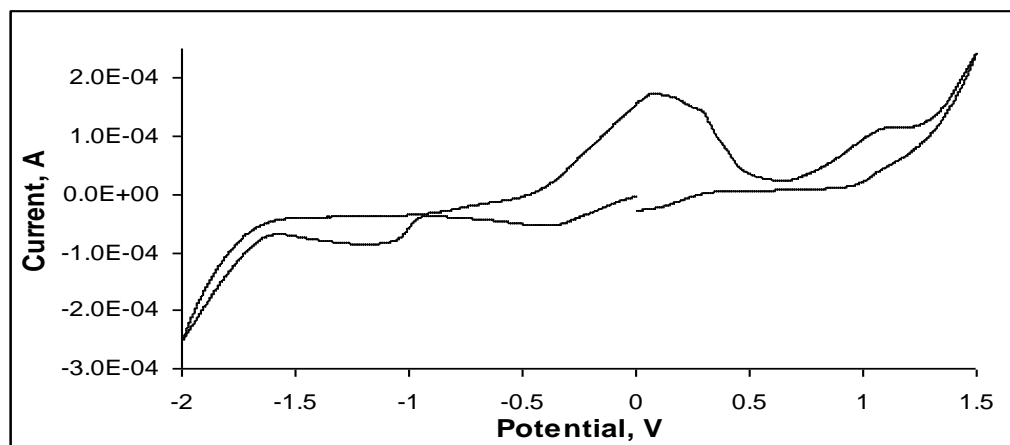
Figure 4.33 CV scanned for Complex 4

The EC mechanism for the redox process of **Complex 4** is shown in **Scheme 4.1**.

$$Cu(II)Cu(II) \xrightarrow{-0.40 \text{ V}} Cu(II)Cu(I) \xrightarrow{-1.18 \text{ V}} Cu(I)Cu(I)$$

$$Cu(I)Cu(I) \longrightarrow 2\,Cu(I) \xrightarrow{+0.31 \text{ V}} 2\,Cu(II)$$

disproportionation

$$Cu(0) + Cu(II)$$

+0.11 V

$$Cu(II)$$
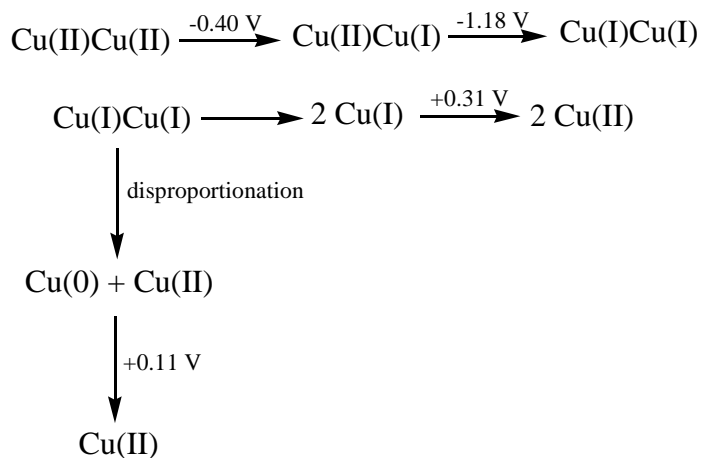
Scheme 4.1 Redox process of Complex 4

(ii) Dark green powder

The dark green powder (**Complex 5**) was obtained from the filtrate on complete removal of the solvent. The results of the elemental analyses are 54.75% C,

7.78% H, and 6.93% N, which are in good agreement with the chemical formula $Cu_2C_{44}H_{63}N_5O_{12}$ (FW = 976.5 g mol^{-1}; 54.07% C, 6.45% H and 7.17% N).

Based on the results of the following instrumental analyses, it is proposed to have the structural formula $[Cu_2(p-H_2NC_6H_4COO)_4(CH_3(CH_2)_{14}COOH)(NH_3)].2H_2O$. Thus, this is not the expected product from the reaction.

The FTIR spectrum (**Figure 4.34)** shows the presence of the expected functional groups. The ΔCOO value is 178 cm^{-1} suggesting bidentate *syn-syn* bridging carboxylate ligand, from which a binuclear complex may be inferred.
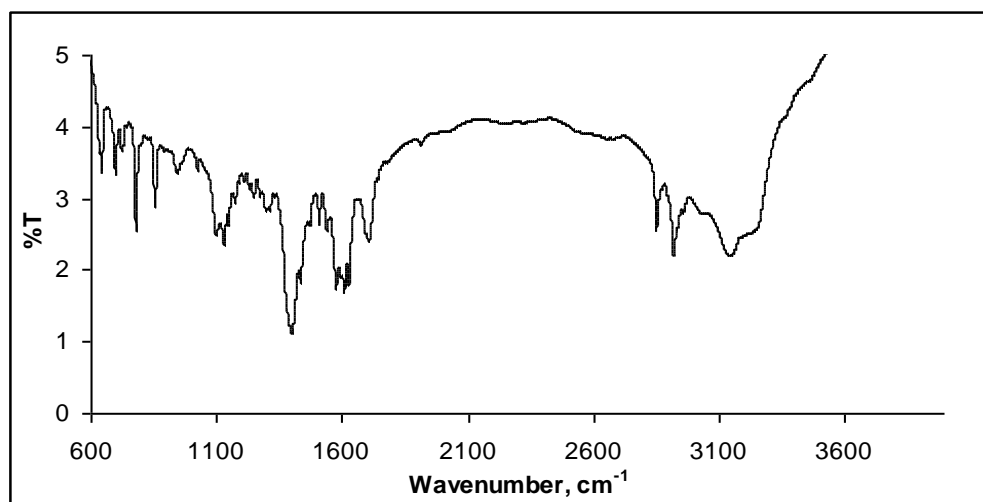
Figure 4.34 *FTIR spectrum of **Complex 5***

The value of Λ_M of **Complex 5** in DMSO-CH₃COOH was 69 S $cm^2 mol^{-1}$. The high value means that the complex is 1:1 electrolyte in solution. This is similar with the previous complexes, which was 1:1 electrolytes in these solvents.

The solid state UV-vis spectrum of **Complex 5** (**Figure 4.35(a)**) shows a broad *d-d* band at 702 nm (Band I). The spectrum of the powder dissolved in DMSO-CH₃COOH (**Figure 4.35(b)**) shows a broad *d-d* peak at 713 nm ($\varepsilon = 617$

$M^{-1}cm^{-1}$) for Band I and a pronounced shoulder at 385 nm ($\varepsilon = 422$ $M^{-1}cm^{-1}$) for Band II. These observations suggest a binuclear complex with square pyramidal geometry at the two copper(II) centres in the solid state, and the geometry is maintained in these solvents.
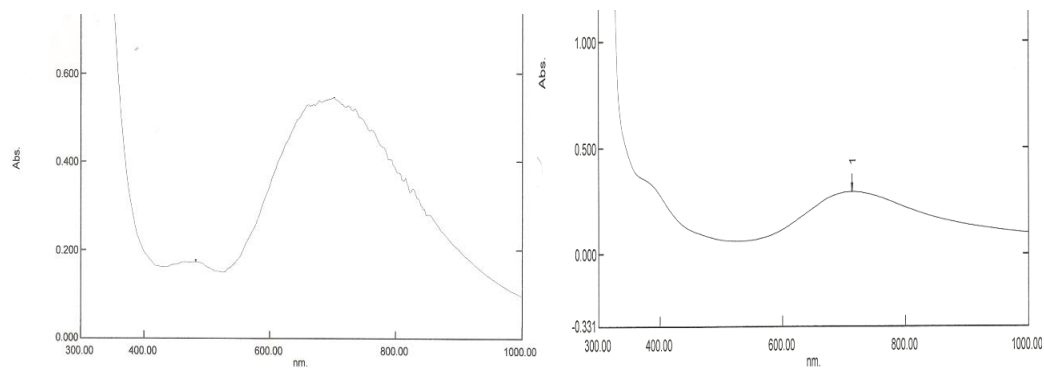
Figure 4.35 *UV spetcra for **Complex 5** as: (a) solid; and (b) solution (DMSO:CH₃COOH)*

Based on all the results discussed above, the proposed structural formula of the **Complex 5** is shown in **Figure 4.36**. The proposed structure is consistent with the chemical formula $Cu_2C_{44}H_{63}N_5O_{12}$ (FW = 976.5 g mol^{-1}) as suggested the elemental analyses, and it shows *syn-syn* bridging carboxylates as suggested from FTIR, and square pyramidal geometry at Cu(II) as suggested from UV-vis.
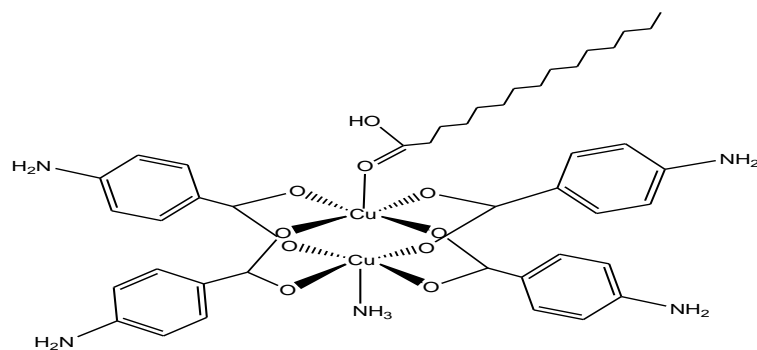
Figure 4.36 *Proposed structural formula of* **Complex 5** *(H$_2$O solvates are not shown)*

The TGA trace (**Figure 4.37**) shows that **Complex 5** is thermally stable up to 217°C. This is slightly lower than **Complex 2** ([Cu$_2$(*p*-H$_2$NC$_6$H$_4$COO)$_4$(H$_2$O)$_2$]) (T$_{decomposition}$ = 257°C). This is consistent with the stronger axial bonds in the former complex, resulting in weaker *p*-NH$_2$C$_6$H$_4$COO-Cu equatorial bonds.

The initial weight loss of 3.0% at about 160°C is assigned to loss of H$_2$O solvates (expected, 3.7%). The next rapid weight loss of 87.2% from 217°C to about 700°C are assigned to loss of NH$_3$, decomposition of *p*-H$_2$NC$_6$H$_4$COO ligands and CH$_3$(CH$_2$)$_{14}$COOH (expected, 83.7%).
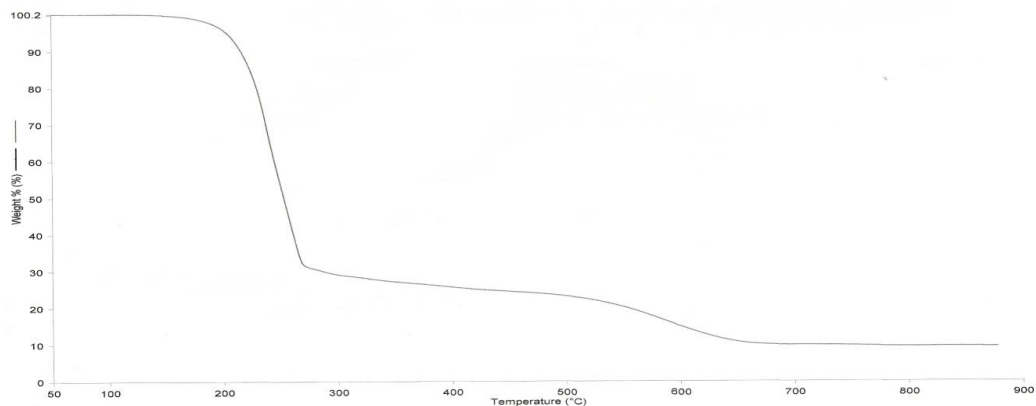
Figure 4.37 *TGA thermogram of* **Complex 5**

The amount of residue above $700^{\circ}C$ is 9.8%. The expected value, assuming that it was CuO, is 16.3%. This may mean weight loss due to volatile copper complex, or that the residue was not purely CuO.

The DSC (**Figure 4.38**) shows a strong endotherm at $65.2^{\circ}C$ ($\Delta H = +52.3$ kJ mol^{-1}) and overlapping endotherms at onset $186^{\circ}C$ ($\Delta H_{combined} = +54.7$ kJ mol^{-1}). The first endotherm is assigned to the melting of axially-coordinated $CH_3(CH_2)_{14}COOH$ (melting point, $62.9^{\circ}C$). The overlapping endotherms, which occurred at about its decomposition temperature ($217^{\circ}C$), are tentatively assigned to the melting of the complex accompanied by its decomposition. Thus, it may be stated that the DSC and TGA results are in good agreement with each other.
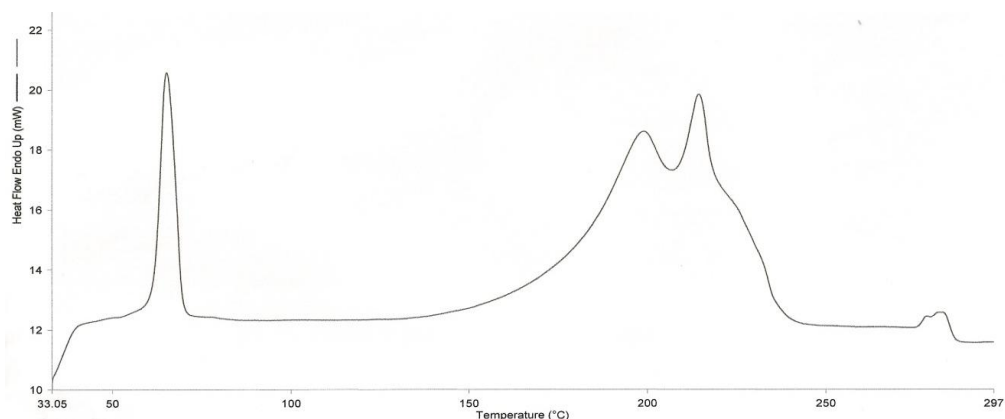
Figure 4.38 *DSC thermogram for **Complex 5***

The POM of **Complex 5** was not recorded as it is not expected to be metallomesogenic, while the room temperature effective magnetic moment (μ_{eff}) cannot be determined due to insufficient sample.

The CV of **Complex 5** (**Figure 4.39**) was scanned cathodically from 0 V in the potential range of -2.0 V to +2.0 V. It shows two reduction peaks at -0.55 V

and -1.05 V, two overlapping oxidation peaks at −0.12 V and +0.07 V, and another broad oxidation peak observed at +1.36 V. The redox process is similar to **Complex 4**, and may be similarly explained.
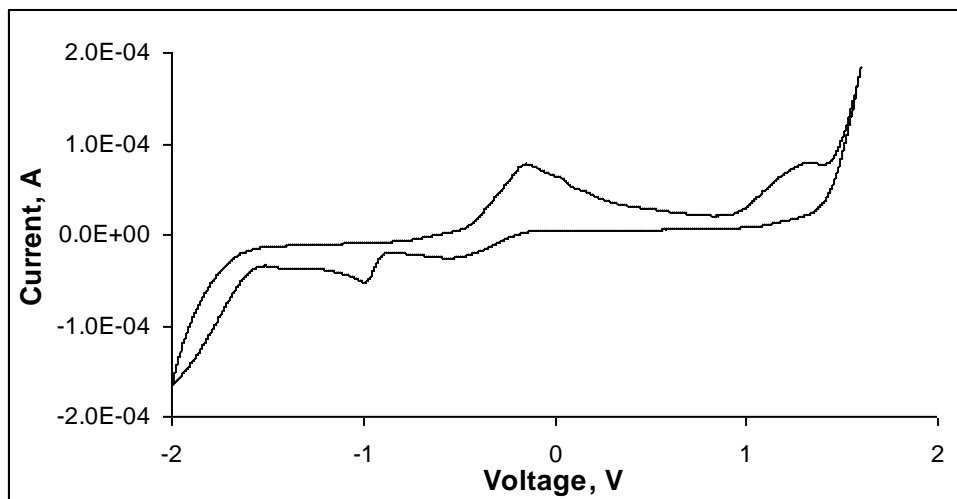
Figure 4.39 *CV for Complex 5*

As a conclusion, the one-pot reaction, using $Cu(NO_3)_2$, $[Cu(CH_3COO)_2]$ and $CuSO_4$, but not $CuCl_2$, was successful to obtain the intended $[Cu_2(p\text{-}H_2NC_6H_4COO)_2(CH_3(CH_2)_{14}COO)_2]$. The complex has low melting temperature, thermally stable, metallomesogenic, magnetic and redox active.

4.3 $[Cu_2(p\text{-}H_3NC_6H_4COO)_n(CH_3(CH_2)_{14}COO)_{4\text{-}n}]$; $n = 1, 3$

The one-pot method was extended for copper(II) complexes with different aromatic:aliphatic carboxylate ratios, namely 1:3 (n =1) and 3:1 (n = 3). The objectives were to study the effect of lower symmetry on the melting temperature and thermal stability of the complex.

4.3.1 [$Cu_2(p\text{-}H_2NC_6H_4COO)(CH_3(CH_2)_{14}COO)_3$]

Two products were isolated from the reaction involving [$Cu(CH_3COO)_2$], p-$H_2NC_6H_4COOH$ and $CH_3(CH_2)_{14}COOH$ in a mole ratio of 2:1:3, specifically a pale blue powder (52.8%) which deposited out of the hot reaction mixture, and a dark green powder obtained on complete removal of the solvent. Accordingly, the analyses were done only for the pale blue powder (**Complex 6**).

The complex was soluble in the same solvents as **Complex 1** ([$Cu_2(p$-$H_2NC_6H_4COO)_2(CH_3(CH_2)_{14}COO)_2].H_2O.CH_3CH_2OH$). The elemental analyses results (60.12% C, 10.83% H, 2.07% N) are in good agreement with the chemical formula $Cu_2C_{59}H_{114}N_2O_{14}$ (FW = 1206.4 g mol^{-1}; 58.7% C, 9.45% H, 2.32% N).

The FTIR spectrum (**Figure 4.40**) shows the presence of the expected functional groups as discussed previously for earlier complexes. The values of ΔCOO are 126, 130 and 155 cm^{-1}, indicating chelating and/or bridging carboxylate ligands.
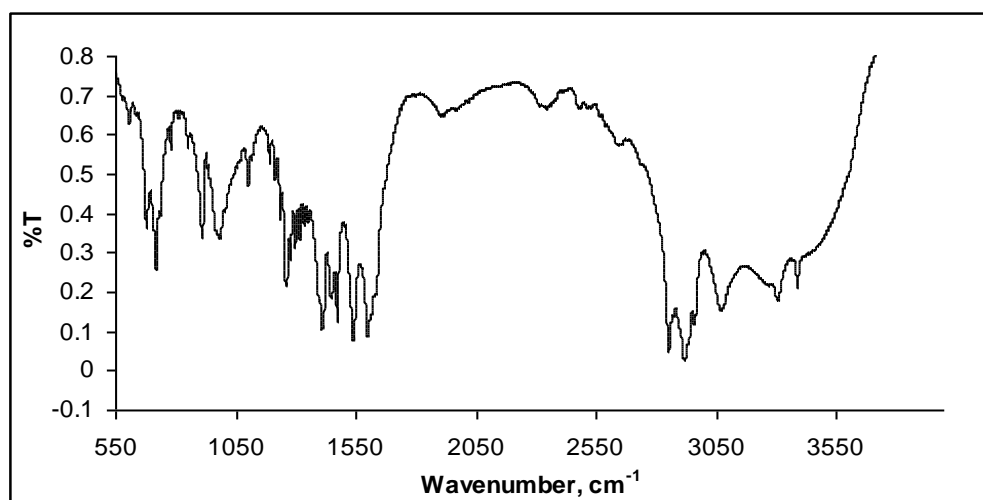
Figure 4.40 *FTIR spectrum of Complex 6*

The value of Λ_M in DMSO-CH$_3$COOH was 20.6 Scm^{2}mol^{-1}. Thus, this complex is also a non-electrolyte similar to most of the more symmetrical complexes discussed above.

The solid state UV-vis spectrum of the complex (**Figure 4.41(a)**) shows two broad *d-d* bands at 667 nm (Band I) and 475 nm (Band II), with absorbance ratio ~ 4:1. The spectrum of the complex dissolved in DMSO-CH$_3$COOH (**Figure 4.41(b)**) shows a broad *d-d* peak at 712 nm (ε = 418 M^{-1}cm^{-1}) for Band I and a weak shoulder at 358 nm (ε = 167 M^{-1}cm^{-1}) for Band II. Thus, the complex is dinuclear and the geometry at Cu(II) is square pyramidal in both solid and solution.
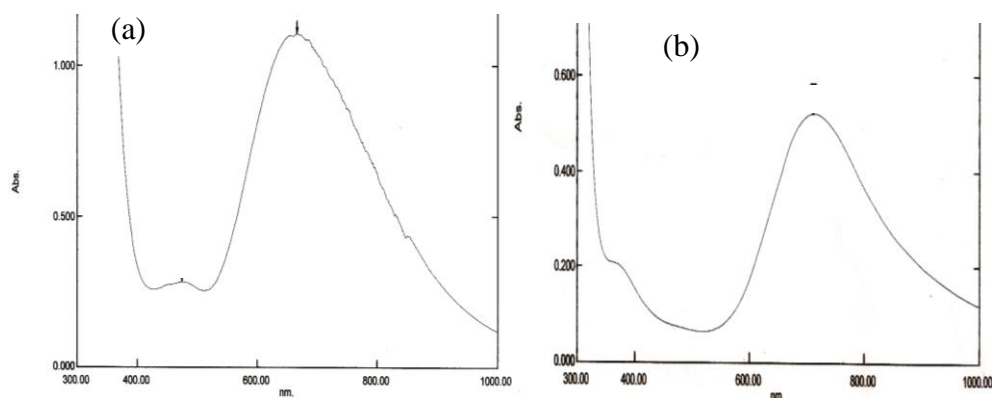
Figure 4.41 The *UV-vis spectra of **Complex 6** as (a) solid; (b) solution (DMSO-CH$_3$COOH)*

Based on the above results, the proposed structural formula of **Complex 6** is [Cu$_2$(*p*-H$_2$NC$_6$H$_4$COO)(CH$_3$(CH$_2$)$_{14}$COO)$_3$(CH$_3$COOH)$_2$].2H$_2$O.NH$_3$ (**Figure 4.42**). The proposed structure is consistent with the chemical formula Cu$_2$C$_{59}$H$_{114}$N$_2$O$_{14}$ (FW = 1206.4 g mol^{-1}) as suggested the elemental analyses,

chelating and bridging carboxylate ligands as suggested from FTIR, and square

pyramidal geometry at Cu(II) as suggested from UV-vis spectroscopy.
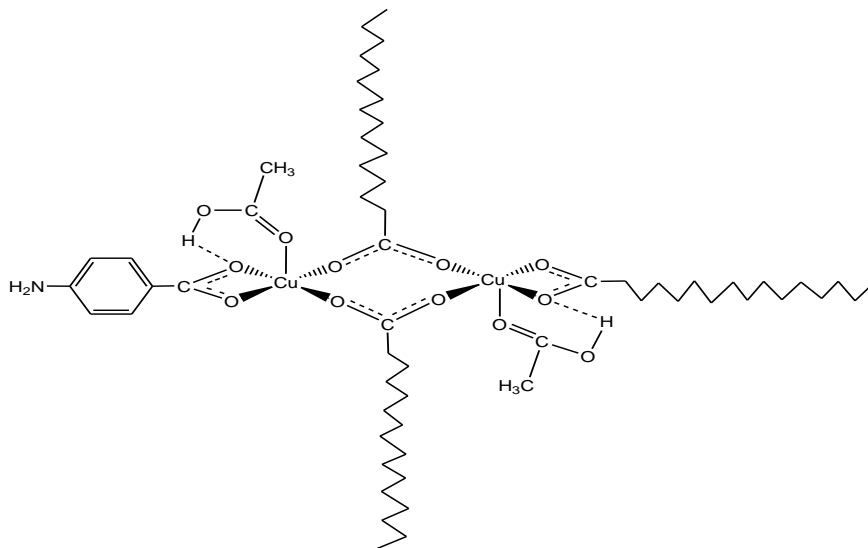
Figure 4.42 *The proposed structural formula for **Complex 6** (solvates H_2O and NH_3 are not shown)*

The TGA trace (**Figure 4.43**) shows that the complex is thermally stable

up to $243^{\circ}C$. Thus, its thermal stability is about the same as the more symmetrical

Complex 1 ($[Cu_2(p\text{-}H_2NC_6H_4COO)_2(CH_3(CH_2)_{14}COO)_2(H_2O)(C_2H_5OH)])$

(**Section 4.2(a)(i)**) ($T_{dec} = 231^{\circ}C$). Actually, **Complex 6** was expected be less

thermally stable as it has a lower proportion of the aromatic carboxylate ligand

(less π back-donation). However, the different structural formulas and the

presence of chelating carboxylates may account for the higher than expected

thermal stability.
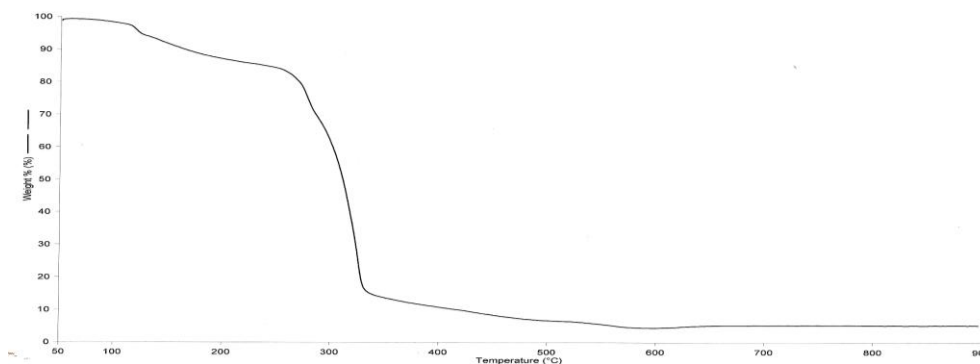
Figure 4.43 *TGA thermogram of Complex 6*

It is further noted that **Complex 6** underwent an initial weight loss of 4.0% from about 50°C to 100°C assigned to evaporation of noncoordinated NH_3 and H_2O molecules (expected 3.2%). The next weight loss from about 100°C to 243°C of 11.2% is assigned to the loss of two coordinated and H-bonded CH_3COOH molecules (expected 11.1%).

The total weight loss from 243°C to 587°C is 78.0% and is assigned to the decomposition of the carboxylate ligands (expected 83.3%) to carbon dioxide and other volatiles. The residue (6.8%) is significantly lower than expected, if assumed CuO, based on the proposed chemical formula (expected 14.9%). Thus, the thermal decomposition of this complex does not follow the same pattern as the previously discussed complexes. The residue may be a mixture of CuO and Cu_2O.

The DSC (**Figure 4.44**) shows two overlapping endotherms at peak temperature of 119°C ($\Delta H_{combined} = +238$ kJ mol^{-1}) assigned to concurrent breaking of H-bond at the aromatic ligand and the van der Waals forces of the aliphatic ligands as the complex melted. This is followed by a broader and weaker

endotherm at 269°C (ΔH = +85 kJ mol^{-1}) assigned to the decomposition of the carboxylate ligands.
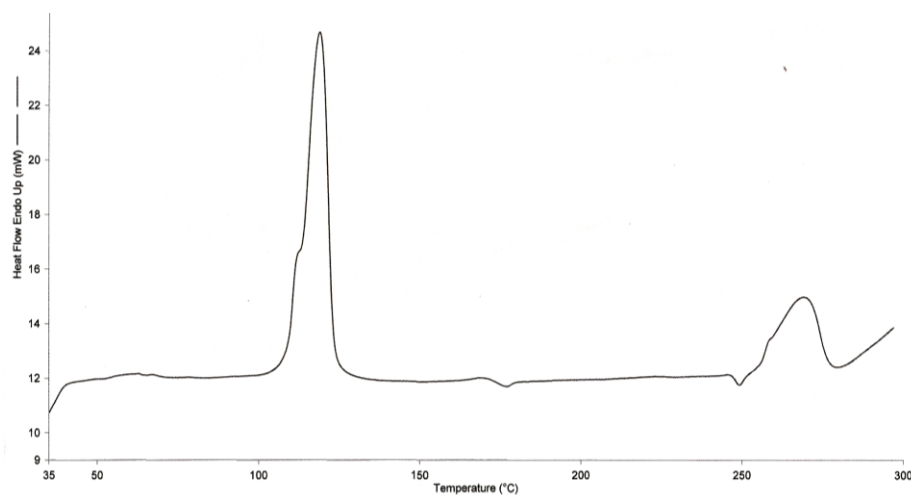
Figure 4.44 *DSC thermogram of* **Complex 6**

It is again noted that these values are comparable with **Complex 1** ([Cu$_2$(*p*-H$_2$NC$_6$H$_4$COO)$_2$(CH$_3$(CH$_2$)$_{14}$COO)$_2$(H$_2$O)(C$_2$H$_5$OH)]) (116°C, ΔH = +201 kJ mol^{-1}; 266°C, ΔH = +75 kJ mol^{-1}) respectively. The melting temperature of **Complex 6** is expected to be lower as it has a lower symmetry. However, the different geometry and the presence of additional long alkyl chain seem to counteract the symmetry effect.

From POM, **Complex 6** was observed to melt at 115°C and then cleared to an isotropic liquid at 160°C (**Figure 4.45 (a)**). The colour of the liquid darkened on further heating to temperatures below its decomposition temperature. On cooling from the isotropic liquid phase, a smectic C mesophase, SmC [47] was observed at about 70°C (**Figure 4.45 (b)**) and remained unchanged on further cooling to room temperature.

(a)   (b)
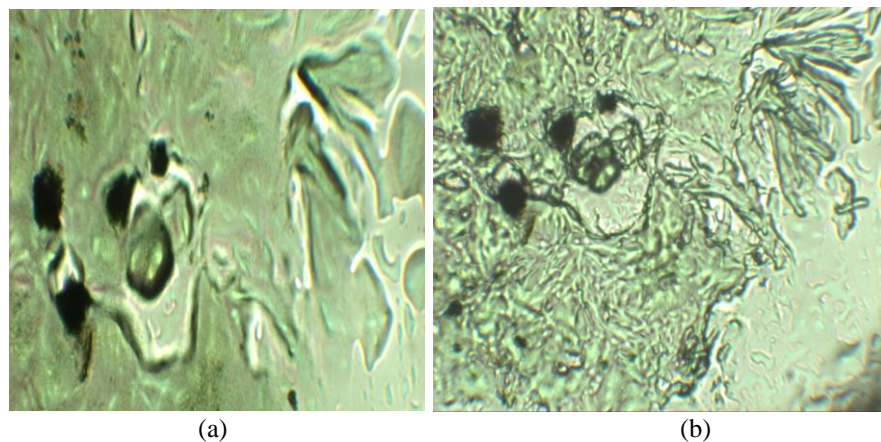
Figure 4.45 *POM of **Complex 6** on (a) heating at 160ºC (clearing temperature) and (b) cooling at about 70 ºC*

The μ_{eff} value for **Complex 6** at room temperature is 3.50 B.M. The -2J value is 122 cm^{-1}. Thus, it may be concluded that there exists as antiferromagnetic interaction between the two copper(II) centre in the complex.

The CV shows two reduction peaks at -0.71 V and -0.99 V, and two overlapping oxidation peaks at –0.03 V and +1.23 V (**Figure 4.46**). The peak separations (ΔE) are 0.68 V and 0.96 V, and the corresponding ratios of the anodic and cathodic peak currents (I_{pa}/I_{pc}) are 1.4 and 2.1. These are similar to **Complex 1**, and may be similarly explained.
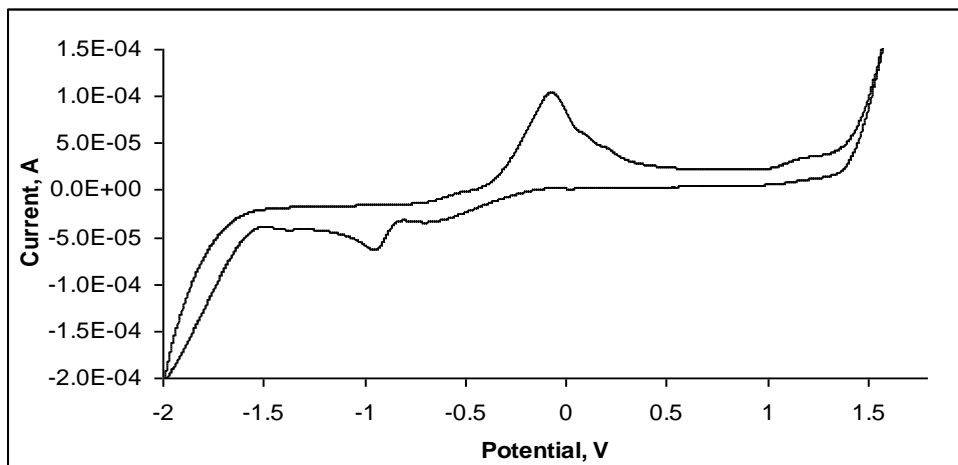
Figure 4.46 *CV scanned of* **Complex 6**

To summarise, the one-pot reaction was successful to obtain the intended $[Cu_2(p\text{-}H_2NC_6H_4COO)(CH_3(CH_2)_{14}COO)_3(CH_3COOH)_2].2H_2O.NH_3$. Its geometry, melting temperature, thermal stability, and metallomesogenic, magnetic and redox properties were similar to ($[Cu_2(p\text{-}H_2NC_6H_4COO)_2(CH_3(CH_2)_{14}COO)_2(H_2O)(C_2H_5OH)]$).

4.3.2 $[Cu_2(p\text{-}H_2NC_6H_4COO)_3(CH_3(CH_2)_{14}COO)]$

Two products were isolated from the reaction involving $[Cu(CH_3COO)_2]$, p-$H_2NC_6H_4COOH$ and $CH_3(CH_2)_{14}COOH$ in a mole ratio of 2:3:1: (a) a dark green powder (15.5%) and (b) a pale blue powder (39.4%).

(a) Dark green powder

The dark green powder was the residue from the hot reaction mixture. Based on the following analytical evidence, the powder is actually **[Complex 3].**$3H_2O$ (chemical formula, $[Cu_2(p\text{-}H_2NC_6H_4COO)_3(CH_3(CH_2)_{14}COO)(H_2O)(NH_3)].3H_2O$ (**Section 4.2(b)(i)**).

The results of the elemental analyses (50.05% C, 5.34% H, and 6.65% N) are in good agreement with the chemical formula $Cu_2C_{37}H_{60}N_4O_{12}$ (FW = 879.5 g mol^{-1}; 50.48% C, 6.88% H and 6.37% N). The FTIR spectrum (**Figure 4.47**) and UV-vis spectra in both the solid state and in solution (**Figure 4.48** are similar to that of **Complex 3.**
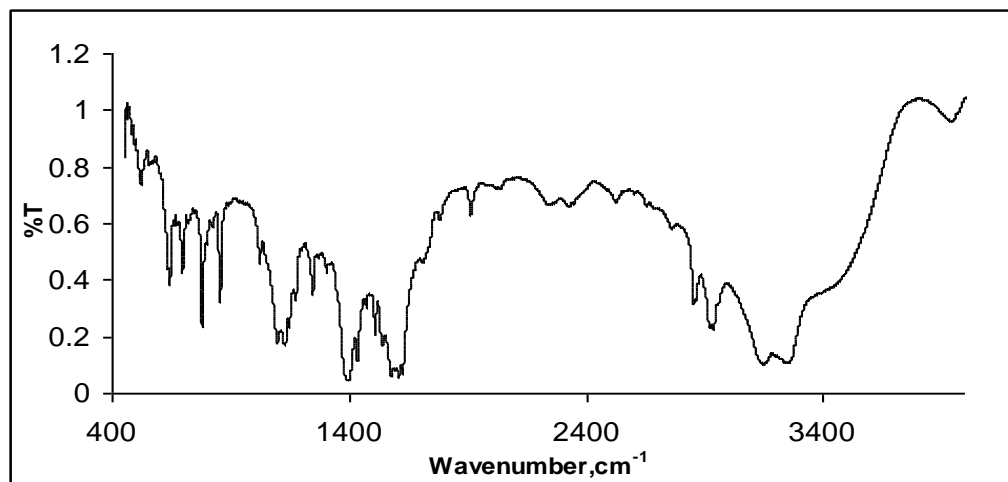
Figure 4.47 *FTIR spectrum of dark green powder*
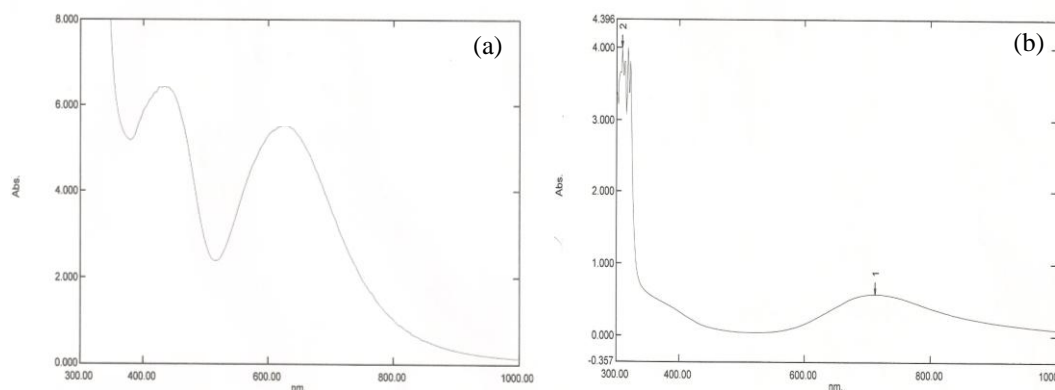
Figure 4.48 *UV-vis spectra of dark green powder (a) solid; and (b) solution (DMSO-CH₃COOH)*

(a) Pale blue powder

The pale blue powder deposited out of the filtrate on standing at room temperature for a few day.

Based on the following analytical evidence, the powder is actually **Complex 1** [Cu$_2$(p-H$_2$NC$_6$H$_4$COO)$_2$(CH$_3$(CH$_2$)$_{14}$COO)$_2$(H$_2$O)(CH$_3$CH$_2$OH)] (**Section 4.2(a)(i)**).

The results of the elemental analyses (59.80% C, 11.66% H, and 2.14% N) are in good agreement with the chemical formula Cu$_2$C$_{37}$H$_{60}$N$_4$O$_{12}$ (FW = 879.5 g mol^{-1}; 59.24% C, 10.92% H and 2.28% N). The FTIR spectrum (**Figure 4.49)** and UV-vis spectra in both the solid state and in solution (**Figure 4.50)** are similar to that of **Complex 1.**
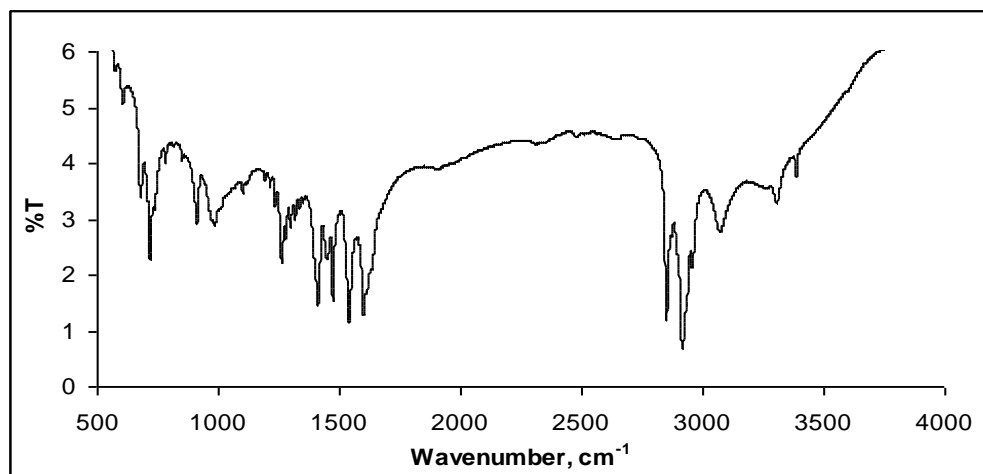
Figure 4.49 *FTIR spectrum of pale blue powder*
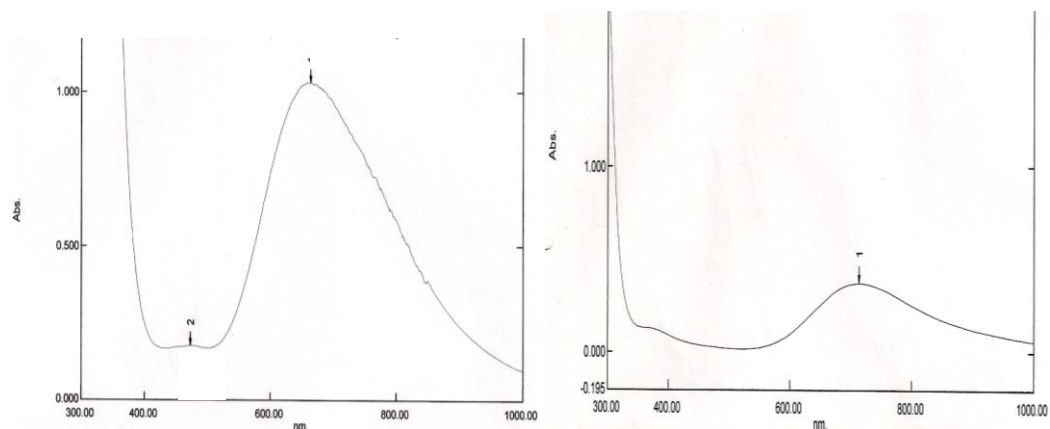
Figure 4.50 *UV-Vis spectra of pale blue powder as (a) solid; and (b) solution (DMSO:CH₃COOH)*

To summarise, the one-pot reaction was successful to obtain the intended $[Cu_2(p\text{-}H_2NC_6H_4COO)_3(CH_3(CH_2)_{14}COO)(H_2O)(NH_3)].3H_2O$ (**Complex 3**) formed as the residue. The complex did not melt, thermally stable, ferromagnetic and redox active.

REFERENCES

[1]   J. Lewis and F. Mabbs, Notes, 1965, 3894 – 3897

[2]   W. E. Hatfield, C. S. Fountain, and R. Whyman, *Inorganic Chemistry*, Vol. 5, No. 11, 1966, 1855-1858

[3]   F. Cariati, L. Erre, G. Micera, A. Panzanelli, and P. Piu, *Thermochimica Acta,* 66 (1983) 1 – 10

[4]   M. Inoue, M. Kishita, and M. Kubo, Inorganic Chemistry, Vol. 3, No. 2, 1964, 239–242

[5]   F. Cariati, L. Erre, G. Micera, A. Panzanelli, G. Ciani, and A. Sironi, *Inorganica Chimica Acta*, 80 (1983) 57-65

[6]   S.P. Perlepes, E.Libby, W. E. Streib, K. Folting and G. Christou, *Polyhedron* Vol. 11, No. 8, pp 923-936, 1992

[7]   W.J.Geary, *Coordination Chemistry Review*, Vol. 7, 1971, 81-122

[8]   A. Garcis-Raso, J.J. Fiol, F. Badenas, E. Lago, E. Molins. *Polyhedron*, **20,** 2877 (2001).

[9]   R. Cejudo, G. Alzuet, J. Borras, M. Liu-Gonzalez, F. Zanz-Ruiz. *Polyhedron*, **21,** 1057 (2002).

[10]   G.S. Siluvai, N.N. Murthy, *Polyhedron*, **28,** 2149 (2009).

[11]   C. Yenikaya, M. Poyraz, M. Sari, F. Demirci, H. Ilkimen, O. Buyukgungor, *Polyhedron*, **28,** 3526 (2009).

[12]   M. Kato, H. B. Jonassen, J. C. Fanning. *Chem. Rev*., **64,** 99 (1964).

[13]   V.T. Yilmaz, Y. Topcu, F. Yilmaz, C. Thoene. *Polyhedron*, **20,** 3209 (2001).

[14]   B.K. Koo. *Bull. Korean Chem. Soc*., **22(1)**, 113 (2001).

[15]   X. Liu, E.J.L. McInnes, C.A. Kilner, M. Thornton-Pett, M.A. Halcrow. *Polyhedron*, **20,** 2889 (2001).

[16]   E. Kokot, R.L. Martin, *Inorg. Chem*., **3,** 1306 (1964).

[17]   E. Kavlakoglu, A. Elmali, Y. Elerman, I. Svoboda. *Polyhedron*, **21,** 1539 (2002).

[18]   A.N.C.Mat, H.Khaledi, J.T.Tee, N.Abdullah, *5th International Conference on Surfaces, Coating & Nanostructures Materials (NANOSMAT-5)*, Reims, France, 19-21 October 2010

[19]   M. I. Mohamadin, N. Abdullah. *Central European Journal of Chemistry*, **8**, 1090 (2010)

[20]   F.Q. Wang, D.F. Weng, X.J. Zheng, J.J. Zhang, H. Mad, L.P. Jin. *Inorg. Chim. Acta,* **360,** 2029 (2007).

[21]   F. Cariati, L. Erre, G. Micera, A. Panzanelli, P. Piu. *Thermochim. Acta*, **66,** 1 (1983).

[22]   C. Yenikaya, M. Poyraz, M. Sari, F. Demirci, H. Ilkimen, O. Buyukgungor. *Polyhedron,* **28,** 3526 (2009).

[23]   C-T Liao, Y-J Wang, C-S Huang, H-S Sheu, G-H Lee, C.K. Lai. *Tetrahedron*, **63,** 12437 (2007).

[24]   F. Hanic, J. Michalov. *Acta Cryst*., **13**, 299 (1960).

[25]   G. S. Attard, P. R. Cullum. *Liq. Cryst*., **8(3)**, 299 (1990).

[26] S. Konar, S. C. Manna, E. Zangrando, N. R. Chaudhuri, *Inorganica Chimica Acta*, doi:10.1016/j.ica.2003.12.003.

[27] A.M. Sosa, V.M. Ugalde-Saldívar, I. Gonzålez, L. Gasque, *J. Electroanal. Chem*., **579**, 103 (2005).

[28] A.Karadag, V.T.Yilmaz, C.Thoene, *Polyhedron*, 20 (2001) 635-641